INTEGRATIVE COMPUTATIONAL ANALYSIS OF CFTR MUTATIONS LINKED TO CYSTIC FIBROSIS

BILAL, I.[1] – SARDAR, N.[2] – ISLAM, A.[2] – NOMAN, A.[3*] – RAMZAN, K.[1] – PARVEEN, M.[4] – WAHEED, A.[1] – ALI, M. Z.[2]

[1] *Department of Biochemistry, University of Okara, Okara, Pakistan.*

[2] *Department of Microbiology and Molecular Genetics, University of Okara, Punjab, Pakistan.*

[3] *Department of Zoology, University of Okara, Punjab, Pakistan.*

[4] *Department of Molecular Biology, University of Okara, Punjab, Pakistan.*

**Corresponding author*
e-mail: alinoman1907[at]gmail.com

(Received 14th July 2025; revised 02nd November 2025; accepted 19th November 2025)

Abstract. The CFTR gene encodes a chloride channel essential for epithelial ion transport, and deleterious nsSNPs are a major cause of cystic fibrosis (CF). CF is an autosomal recessive disorder affecting multiple systems, with symptoms including chronic cough, recurrent lung infections, bronchiectasis, reduced pulmonary function, pancreatic insufficiency, malabsorption, poor growth, salty-tasting skin, male infertility, liver disease, and diabetes. To date, over 4,000 CFTR mutations have been reported, with F508del being the most common, accounting for nearly 70% of cases. This study aimed to identify deleterious nsSNPs in the CFTR gene and evaluate their structural and functional impact using an integrative in silico pipeline. Additionally, molecular docking was performed to explore potential therapeutic modulators for cystic fibrosis. The NCBI database reported over 282,000 SNPs in CFTR, of which SNPnexus analysis identified 132 nsSNPs as highly deleterious. Furthermore, 30 nsSNPs were consistently predicted to be deleterious across 15 computational tools. Notably, variants such as I105N, K273Q, and G1249R demonstrated destabilizing effects, with RMSD values ranging from 0.93 to 0.98 Å, indicating substantial conformational alterations. Molecular docking revealed strong ligand interactions with both wild-type and mutant CFTR, particularly for apoptozole, Congo Red, NAD, melanin, and cAMP, while repurposed drugs such as nelfinavir and amprenavir demonstrated favorable binding, supporting their potential to rescue misfolded proteins. This integrative in silico study highlights 30 pathogenic CFTR nsSNPs with destabilizing structural effects and identifies potential modulators, providing a robust framework for experimental validation, drug repurposing, and personalized therapeutic strategies in cystic fibrosis.
Keywords: *Apoptozole, cystic fibrosis, drug discovery, molecular docking, structural modeling*

Introduction

Cystic fibrosis (CF) is an autosomal recessive disorder caused by mutations in the cystic fibrosis transmembrane conductance regulator (CFTR) gene, with over 4000 variants identified (Ideozu et al., 2024; Rafique et al., 2024). The CFTR protein functions as a chloride channel, regulating ion balance to maintain thin mucus and proper epithelial hydration. CF leads to thick mucus, causing chronic lung infections, pancreatic insufficiency, malabsorption, poor growth, and infertility (Purushothaman and Nelson, 2023). CFTR mutations are grouped into six classes (I–VI) based on their effects on protein production, folding, trafficking, and stability. Missense mutations are most common. Classes I–III abolish function, causing severe disease, while Classes IV–VI retain partial activity with milder symptoms. Notable mutations include G542X

(Class I), F508del (Class II), and G551D (Class III) (Ramananda et al., 2024; Deletang and Taulan-Cadars, 2022). Additionally, polymorphism in CFTR coding and regulatory regions affect its expression and function, contributing to clinical variability (Parisi et al., 2022). The CFTR gene, mapped on chromosome 7q31.2 (NC_000007.14), spans about 190 kb and contains 27 exons encoding a 6.5 kb mRNA that translates into a 1,480–amino acid protein. After folding and glycosylation in the endoplasmic reticulum, it traffics through the Golgi to the apical membrane, where it mediates chloride and bicarbonate transport. Structurally, CFTR belongs to the ATP-binding cassette (ABC) transporter family and is composed of two membrane-spanning domains (MSD1 and MSD2) that form the channel, two nucleotide-binding domains (NBD1 and NBD2) that regulate ATP-driven gating, and a regulatory (R) domain that controls channel activity. Moreover, CFTR also transports glutathione, contributing to epithelial homeostasis (Zhang et al, 2025; Ideozu et al., 2024).

Over 1,900 CFTR variants have been described, with ~1,500 linked to disease (Mathew et al., 2021). The ΔF508 variant, present in over 70% of cases, disrupts CFTR folding and trafficking, impairing chloride transport. This causes thick secretions that affect the respiratory, digestive, and reproductive systems, with lung complications being the leading cause of morbidity and mortality (George Priya Doss et al., 2008). Moreover, CFTR is a phosphorylation-regulated by protein kinase A or C, enabling ATP binding and channel opening, allowing chloride flow with sodium and water. Disruption impairs mucociliary clearance and fluid balance, leading to complications such as diarrhea or constipation. Moreover, missense mutations in CFTR can disrupt transcription factor binding, regulatory elements, or splicing enhancers, thereby altering gene expression. This study employed an in-silico approach to assess the impact of nsSNPs on CFTR structure and function. Homology modeling and virtual screening were used to explore ligand interactions, revealing variant-induced destabilization. These findings advance understanding of cystic fibrosis pathogenesis and support future therapeutic development.

Materials and Methods

Mining datasets

The CFTR protein sequence was obtained from UniProtKB and the NCBI database. For computational analysis, the complete SNP dataset of the human CFTR gene was retrieved from dbSNP-NCBI, and the overall methodology is presented in *Figure 1*.

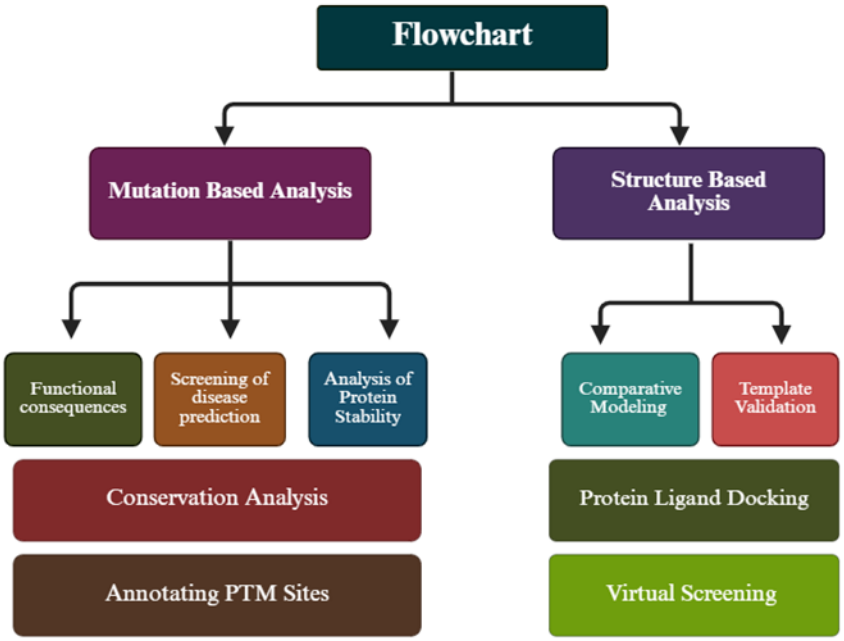

Figure 1. *Schematic representation of the CFTR gene workflow used in this study.*

Bioinformatics tools for nsSNP analysis

Several bioinformatics tools were employed to analyze nsSNPs obtained from the dbSNP database. SNPnexus integrates multiple prediction algorithms, including SIFT and PolyPhen. SNAP2 evaluates the functional impact of polymorphisms using the FASTA sequence as input, enabling genome-wide comparisons. PROVEAN applies alignment-based scoring, with variants scoring below -2.5 considered deleterious. PolyPhen-2 predicts substitution effects on a scale from 0 (benign) to 1 (damaging). CADD provides integrative annotations for genome variants, including point mutations and indels. CONDEL classifies nsSNPs as either neutral (0) or deleterious (Ideozu et al., 2024; Tariq et al., 2024; Waheed et al., 2024). The SNPs & GO tool evaluates amino acid substitutions at specific protein sites using Uniprot ID and mutation position as input. Meta-SNP predicts SNVs with an accuracy of ~79%; scores >0.5 are considered damaging (Hasnain et al., 2020; Venkata Subbiah et al., 2020; AbdulAzeez and Borgio, 2016; Magesh and George Priya Doss, 2014). P-MUT predicts the pathological impact of mutations with ~80% accuracy and provides access to all single amino acid variants for disease association analysis (López-Ferrando et al., 2017). PhD-SNP achieves ~78% accuracy and uses a 0–9 scoring scale to assess disease-related mutations (Abuzaid et al., 2024).

Prediction of protein stability alterations

The stability effects of CFTR mutations were assessed by predicting changes in free energy. MUpro estimates ΔΔG values, where scores ≤0 indicate decreased protein stability. I-Mutant 3.0 predicts stability alterations with ~77% accuracy (20, 21). i-Stable uses support vector machine (SVM) algorithms to evaluate the impact of amino acid substitutions on protein stability (Waheed et al., 2024).

Conservation analysis and PTM sites

Evolutionary conservation of CFTR amino acid residues was assessed using ConSurf. Conservation scores ranged from 1 to 9, with values 1–3 indicating variable regions, 4–6 moderate conservation, and 7–9 highly conserved sites (Hasnain et al., 2020; Venkata Subbiah et al., 2020; Armon et al., 2001). PTM analysis was conducted to evaluate the potential effects of CFTR variants on protein regulation through modifications such as phosphorylation, acetylation, methylation, and ubiquitination (Hasan and Khatun, 2018). Phosphorylation sites in the CFTR protein were predicted using MusiteDeep, with the amino acid sequence provided as input (Wang et al., 2020; Chandrasekaran et al., 2017).

Structural modeling and validation

The CFTR protein structure was modeled using SWISS-MODEL, and specific mutations were introduced using PyMOL (Bilal et al., 2025a; 2025b). The models were refined with ModRefiner to optimize geometry and stereochemistry. Model quality was assessed via the SAVES server (https://saves.mbi.ucla.edu), which integrates PROCHECK, ERRAT, and Verify3D (Heidarinia et al., 2025). The Ramachandran plot is generated using the Ramplot server evaluates backbone torsion angles (φ, ψ) to ensure proper stereochemistry (Kumar and Rathore, 2025). Finally, the overall reliability of the predicted structure was verified using QMEAN, which calculates a composite score based on local geometry, long-range interactions, and solvation energy; a Z-score near zero indicates high structural quality (Ramzan and Noman, 2024). Moreover, Structural deviations between wild-type and mutant models were compared using TM-align, with RMSD values used to quantify conformational differences. The structural effects of amino acid substitutions were analyzed using the HOPE server, which evaluates changes in size, charge, and hydrophobicity, considering conserved regions and functional domains to predict impacts on protein stability and function (Kumari et al., 2025; Rasheed et al., 2025).

Virtual screening and molecular docking

Virtual screening was conducted to identify potential ligands interacting with CFTR variants. Ligand structures were retrieved from PubChem and relevant literature. Docking simulations were performed using PyRx, which utilizes AutoDock Vina for protein–ligand docking. Protein and ligand structures were converted to PDBQT format before docking. The interactions of the resulting docked complexes were visualized and analyzed in both 2D and 3D using Discovery Studio Visualizer (Aslam et al., 2024; Ramzan and Noman, 2024; Adeniji et al., 2020).

Results and Discussion

Retrieval of functional SNPs

A total of 282,490 SNPs in the human CFTR gene were retrieved from NCBI dbSNP and analyzed using SNPnexus. Of these, 10,618 were non-synonymous, 233,126 were in coding regions, 32,781 were in the non-coding areas, 2,327 were in untranslated regions, 7,671 were in the 5′ upstream, 6,585 were in the 3′ downstream, and 2,049 were synonymous. Their distribution across the CFTR gene is shown in *Figure 2*. This study emphasizes coding region variants, with non-synonymous SNPs representing a small fraction. For further analysis, we focused on non-synonymous SNPs due to their

potential to change amino acid sequences and affect CFTR protein structure and function. The SIFT algorithm predicted 5,124 SNPs as deleterious and 3,474 as tolerated. PolyPhen identified 4,367 SNPs as potentially damaging (*Figure 3*). Notably, 132 variants were consistently predicted as deleterious by both SIFT (score = 0.00) and PolyPhen (score = 1.00), indicating high deleterious variants (*Table 1*).

Table 1. *SNPnexus predictions of highly deleterious and probably damaging CFTR gene variants.*

VaID	PrCh	SI		PoP		VaID	PrCh	SI		PoP		VaID	PrCh	SI		PoP	
		S	E	S	E			S	E	S	E			S	E	S	E
rs1031657153	P99A	0	D	1	Prob Damage	rs377514639	R258I	0	D	1	Prob Damage	rs1299482973	S707F	0	D	1	Prob Damage
rs397508467	P99L	0	D	1	Prob Damage	rs1296578005	K273Q	0	D	1	Prob Damage	rs397508375	D806G	0	D	1	Prob Damage
rs397508490	L102P	0	D	1	Prob Damage	rs756036343	K273M	0	D	1	Prob Damage	rs757165481	Y849H	0	D	1	Prob Damage
rs397508509	I105N	0	D	1	Prob Damage	rs397508800	W277R	0	D	1	Prob Damage	rs775570582	L165S	0	D	1	Prob Damage
rs397508522	Y109N	0	D	1	Prob Damage	rs151073129	I285F	0	D	1	Prob Damage	rs1402844924	L165F	0	D	1	Prob Damage
rs121909031	Y109C	0	D	1	Prob Damage	rs1204521684	V317G	0	D	1	Prob Damage	rs121909035	H949Y	0	D	1	Prob Damage
rs113993958	D110Y	0	D	1	Prob Damage	rs121909011	R334W	0	D	1	Prob Damage	rs397508444	H949R	0	D	1	Prob Damage
rs140502196	P111L	0	D	1	Prob Damage	rs397508146	L346P	0	D	1	Prob Damage	rs1191342069	G1241D	0	D	1	Prob Damage
rs397508551	N113I	0	D	1	Prob Damage	rs77932196	R347P	0	D	1	Prob Damage	rs397508599	G1244R	0	D	1	Prob Damage
rs761370893	E116G	0	D	1	Prob Damage	rs397508188	L441P	0	D	1	Prob Damage	rs267606723	G1244E	0	D	1	Prob Damage
rs201958172	A120P	0	D	1	Prob Damage	rs121908805	S466L	0	D	1	Prob Damage	rs397508602	G1249R	0	D	1	Prob Damage
rs397508592	Y122H	0	D	1	Prob Damage	rs1800089	L467F	0	D	1	Prob Damage	rs121909040	G1249E	0	D	1	Prob Damage
rs377295859	Y122C	0	D	1	Prob Damage	rs139573311	L467P	0	D	1	Prob Damage	rs117400534	L1253F	0	D	1	Prob Damage
rs397508609	G126D	0	D	1	Prob Damage	rs397508202	L468P	0	D	1	Prob Damage	rs11971167	D1270Y	0	D	1	Prob Damage
rs1162745955	L129H	0	D	1	Prob Damage	rs79282516	G480S	0	D	1	Prob Damage	rs765549490	D1270G	0	D	1	Prob Damage
rs397508674	L137H	0	D	1	Prob Damage	rs397508208	G480D	0	D	1	Prob Damage	rs753920616	F508V	0	D	1	Prob Damage
rs1800078	L138P	0	D	1	Prob Damage	rs200626971	W496C	0	D	1	Prob Damage	rs77010898	W1282C	0	D	1	Prob Damage
rs397508718	G149R	0	D	1	Prob Damage	rs774945680	G500D	0	D	1	Prob Damage	rs77902683	R1283M	0	D	1	Prob Damage
rs397508719	G149E	0	D	1	Prob Damage	rs397508222	I502N	0	D	1	Prob Damage	rs904990724	G1298R	0	D	1	Prob Damage
rs397508723	A155P	0	D	1	Prob Damage	rs397508224	I506S	0	D	1	Prob Damage	rs193922522	G1298A	0	D	1	Prob Damage
rs397508724	S158C	0	D	1	Prob Damage	rs1800092	I506M	0	D	1	Prob Damage	rs121909042	N1303H	0	D	1	Prob Damage
rs397508727	L159S	0	D	1	Prob Damage	rs74571530	F508C	0	D	1	Prob Damage	rs121909042	N1303Y	0	D	1	Prob Damage
rs397508729	Y161D	0	D	1	Prob Damage	rs758745885	D513Y	0	D	1	Prob Damage	rs397508636	N1303I	0	D	1	Prob Damage
rs397508730	Y161S	0	D	1	Prob Damage	rs368516826	C524R	0	D	1	Prob Damage	rs80034486	N1303K	0	D	1	Prob Damage
rs397508736	L165S	0	D	1	Prob Damage	rs1387755887	G545V	0	D	1	Prob Damage	rs201503139	P1306S	0	D	1	Prob Damage
rs80282562	G178R	0	D	1	Prob Damage	rs1469024267	L548P	0	D	1	Prob Damage	rs397508646	D1312G	0	D	1	Prob Damage

Note: VaID=Variation ID; PrCh=Protein Change; SI=SIFT; PoP=PolyPhen; S=Source; E=Effect; D=Deleterious; Prob Damage=Probably Damage.

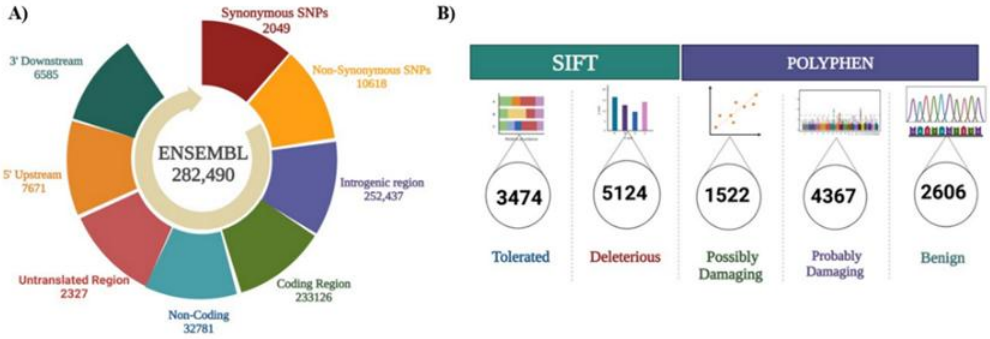

Figure 2. *(A) Donut chart showing the distribution of SNPs across the CFTR gene regions; (B) SIFT and PolyPhen algorithm outcomes.*

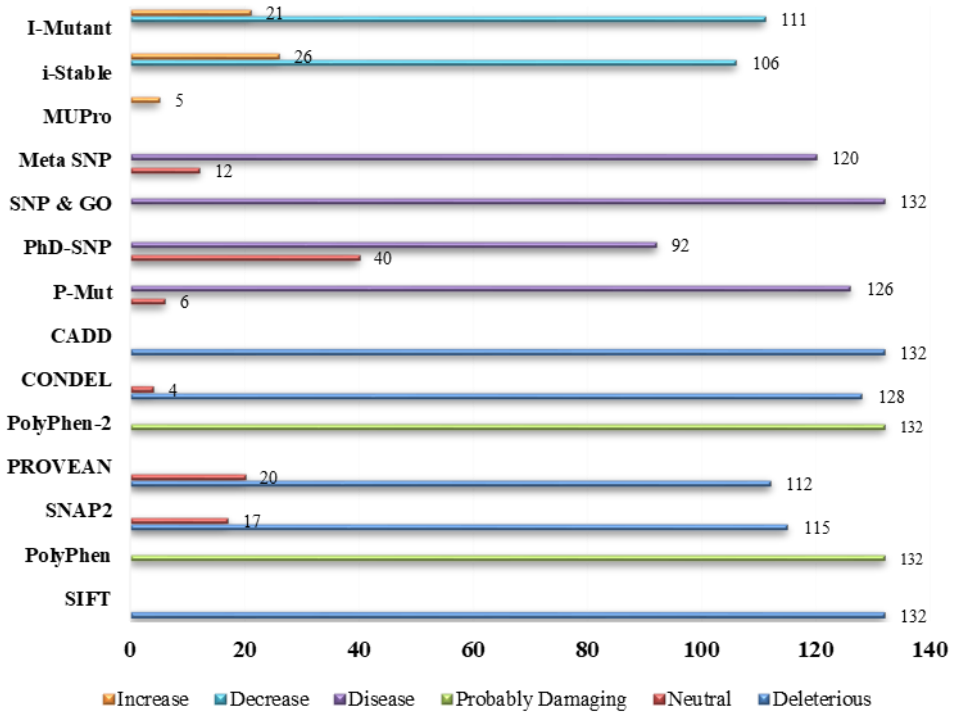

Figure 3. *In silico prediction of CFTR nsSNP functional and stability analysis.*

Annotation of missense SNPs

The analysis of 132 high-confidence CFTR nsSNPs revealed distinct patterns of deleterious and neutral variants across multiple prediction tools (*Table 2*). SNAP2 identified 115 variants as functionally deleterious, while P111L, N113I, S519R, S519I, G551D, R555G, V562I, L564P, F587L, Q590R, D614N, T652A, R668H, S737F, Q768H, L1335F, and I1366M were predicted neutral. PROVEAN classified 112 nsSNPs as deleterious and 20 as neutral, including the same variants plus P574H, L1369F, and D1370H. CADD scores highlighted high pathogenic potential for K273Q, L165S, G1244R, L1356S, G149R, W1282C, G1298R, and R560G, whereas neutral variants scored below 40. ConDEL predictions indicated neutrality for S519I (0.541), S519R (0.462), G551D (0.752), and R555G (0.799). PolyPhen-2 classified all 132 nsSNPs as probably damaging (*Figure 4*). Collectively, these analyses suggest that

these nsSNPs are likely to significantly impact CFTR structure and function. In *Figure 5*, analysis of 132 CFTR nsSNPs revealed that all variants were predicted to be disease-causing by SNP & GO. P-Mut classified most variants as disease-related but identified six variants as neutral, including E116G (0.4718), D192G (0.4395), L467F (0.4722), S519R (0.4215), Q767H (0.4504), and S707F (0.4427). PhD-SNP predicted 40 nsSNPs as neutral, including P111L, N113I, E116G, A120P, Y122H, Y122C, S158C, L159S, L165S, L183I, D192N, D192G, L180F, W216C, G241W, I1267M, L1339F, A1364V, I1366M, H949Y, H949R, G1298A, and P1306S, while the remaining 92 variants were classified as disease-causing. Meta-SNP predicted 12 neutral variants, including P111L, N113I, E116G, S519I, S519R, S707F, I1267M, L1369F, H949Y, Q767H, G1298A, and D1370H, confirming that the majority of nsSNPs are likely pathogenic (*Table 3*).

***Table 2**. Functional predictions of CFTR nsSNPs using SNAP2, PROVEAN, PolyPhen-2, CONDEL, and CADD tools.*

VaID	A.A	SNAP2		PROVEAN		Polyphen-2		CONDEL		C
		E	Sc	E	Sc	E	Sc	Sc 0.522	L	S
rs1031657153	P99A	Effect	75	Deleterious	-6.326	Probably damaging	1	0.689962767	Deleterious	26.5
rs397508467	P99L	Effect	89	Deleterious	-7.86	Probably damaging	1	0.690461493	Deleterious	26.3
rs397508490	L102P	Effect	76	Deleterious	-5.675	Probably damaging	1	0.653429886	Deleterious	27.5
rs397508509	I105N	Effect	96	Deleterious	-4.741	Probably damaging	1	0.639361713	Deleterious	28.5
rs397508522	Y109N	Effect	94	Deleterious	-4.14	Probably damaging	1	0.623628807	Deleterious	26.7
rs121909031	Y109C	Effect	28	Deleterious	-4.045	Probably damaging	1	0.623935753	Deleterious	25.9
rs113993958	D110Y	Effect	95	Neutral	-2.419	Probably damaging	1	0.6461576	Deleterious	26.4
rs140502196	P111L	Neutral	-9	Deleterious	-2.888	Probably damaging	0.997	0.626352695	Deleterious	23.7
rs397508551	N113I	Neutral	-55	Neutral	-2.479	Probably damaging	0.992	0.604836303	Deleterious	24.4
rs761370893	E116G	Neutral	-22	Neutral	-2.237	Probably damaging	1	0.631819172	Deleterious	32
rs201958172	A120P	Effect	90	Neutral	-0.594	Probably damaging	0.999	0.573850662	Deleterious	24.7
rs397508592	Y122H	Effect	5	Neutral	-2.374	Probably damaging	1	0.533685761	Deleterious	26
rs377295859	Y122C	Neutral	-4	Deleterious	-3.155	Probably damaging	1	0.533868225	Deleterious	25.3
rs397508609	G126D	Effect	45	Deleterious	-3.059	Probably damaging	1	0.612333936	Deleterious	27.1
rs1162745955	L129H	Effect	42	Deleterious	-3.805	Probably damaging	1	0.598494635	Deleterious	28
rs397508674	L137H	Effect	74	Deleterious	-4.032	Probably damaging	1	0.584131047	Deleterious	28.4
rs1800078	L138P	Effect	39	Deleterious	-5.019	Probably damaging	1	0.544893044	Deleterious	27.3
rs397508718	G149R	Effect	55	Deleterious	-6.594	Probably damaging	1	0.614160066	Deleterious	38
rs397508719	G149E	Effect	99	Deleterious	-6.559	Probably damaging	1	0.613969807	Deleterious	31
rs397508723	A155P	Effect	69	Deleterious	-3.221	Probably damaging	1	0.622122435	Deleterious	27.4
rs397508724	S158C	Neutral	-14	Deleterious	-3.24	Probably damaging	1	0.54546275	Deleterious	27.6
rs397508727	L159S	Effect	9	Neutral	-1.388	Probably damaging	1	0.590006845	Deleterious	40
rs397508729	Y161D	Effect	93	Deleterious	-8.82	Probably damaging	1	0.625738666	Deleterious	28.3
rs397508730	Y161S	Effect	86	Deleterious	-7.937	Probably damaging	1	0.625908003	Deleterious	29.4
rs397508736	L165S	Effect	70	Deleterious	-5.076	Probably damaging	1	0.624026793	Deleterious	37
rs80282562	G178R	Effect	39	Deleterious	-6.597	Probably damaging	1	0.623460666	Deleterious	39
rs397508748	G178E	Effect	96	Deleterious	-6.484	Probably damaging	1	0.623444642	Deleterious	28.9
rs397508751	L183I	Effect	13	Neutral	-1.298	Probably damaging	1	0.597193052	Deleterious	25.6
rs766640075	L188P	Effect	79	Deleterious	-2.737	Probably damaging	1	0.572304299	Deleterious	29.9
rs397508756	D192N	Effect	94	Neutral	-1.17	Probably damaging	1	0.628164312	Deleterious	32
rs397508758	D192G	Effect	94	Neutral	-2.456	Probably damaging	1	0.59406821	Deleterious	31
rs755405930	E193G	Effect	96	Deleterious	-3.525	Probably damaging	1	0.541998905	Deleterious	34
rs376008630	G194R	Effect	76	Neutral	-0.823	Probably damaging	1	0.536433678	Deleterious	45
rs397508765	H199Q	Effect	21	Deleterious	-3.161	Probably damaging	1	0.630271618	Deleterious	23.7
rs1457675231	F200S	Effect	64	Deleterious	-2.767	Probably damaging	1	0.598710441	Deleterious	31
rs121908803	P205S	Neutral	-9	Deleterious	-6.506	Probably damaging	1	0.62711446	Deleterious	24.7
rs397508769	P205R	Effect	98	Deleterious	-7.354	Probably damaging	1	0.626471433	Deleterious	25.3
rs121908752	L206W	Effect	42	Deleterious	-3.158	Probably damaging	1	0.602951749	Deleterious	38
rs1227994401	Q207H	Effect	71	Deleterious	-4.163	Probably damaging	1	0.589974325	Deleterious	23.3
rs759719664	L180F	Effect	30	Neutral	-2.338	Probably damaging	1	0.54889768	Deleterious	24

rs397508776	W216C	Effect	14	Deleterious	-7.936	Probably damaging	1	0.587346356	Deleterious	39
rs770891254	G226E	Effect	74	Deleterious	-6.071	Probably damaging	1	0.604404997	Deleterious	25.9
rs397508785	Q237H	Effect	55	Neutral	-2.07	Probably damaging	1	0.629183694	Deleterious	23.4
rs397508789	G241W	Effect	92	Deleterious	-3.354	Probably damaging	1	0.588153323	Deleterious	28.6
rs377514639	R258I	Effect	96	Deleterious	-4.712	Probably damaging	1	0.632108701	Deleterious	29.5
rs1296578005	K273Q	Effect	77	Deleterious	-3.396	Probably damaging	1	0.624575021	Deleterious	41
rs756036343	K273M	Effect	82	Deleterious	-5.094	Probably damaging	1	0.62411619	Deleterious	28
rs397508800	W277R	Effect	82	Deleterious	-11.885	Probably damaging	1	0.634257459	Deleterious	29.3
rs151073129	I285F	Neutral	-65	Deleterious	-2.77	Probably damaging	1	0.609117124	Deleterious	27.8
rs1204521684	V317G	Effect	51	Deleterious	-3.084	Probably damaging	1	0.543605135	Deleterious	27.7
rs121909011	R334W	Effect	96	Deleterious	-3.421	Probably damaging	1	0.540073147	Deleterious	24.7
rs397508146	L346P	Effect	55	Deleterious	-4.152	Probably damaging	1	0.611034144	Deleterious	29.1
rs77932196	R347P	Effect	58	Neutral	-0.718	Probably damaging	1	0.618903437	Deleterious	30
rs397508188	L441P	Effect	86	Deleterious	-5.288	Probably damaging	1	0.682955987	Deleterious	28.6
rs121908805	S466L	Effect	89	Deleterious	-5.025	Probably damaging	1	0.585878446	Deleterious	38
rs1800089	L467F	Effect	21	Deleterious	-2.687	Probably damaging	1	0.564902727	Deleterious	24.6
rs139573311	L467P	Effect	97	Deleterious	-5.874	Probably damaging	1	0.761524877	Deleterious	28.2
rs397508202	L468P	Effect	75	Deleterious	-5.83	Probably damaging	1	0.734640484	Deleterious	28.5
rs79282516	G480S	Effect	95	Deleterious	-5.046	Probably damaging	1	0.734211973	Deleterious	28.5
rs397508208	G480D	Effect	98	Deleterious	-5.978	Probably damaging	1	0.744839813	Deleterious	26.7
rs200626971	W496C	Effect	25	Deleterious	-11.907	Probably damaging	1	0.667176959	Deleterious	40
rs774945680	G500D	Effect	86	Deleterious	-3.722	Probably damaging	1	0.548933512	Deleterious	26.9
rs397508222	I502N	Effect	81	Deleterious	-5.352	Probably damaging	1	0.678737274	Deleterious	28.2
rs397508224	I506S	Effect	97	Deleterious	-5.235	Probably damaging	1	0.740253168	Deleterious	28
rs1800092	I506M	Effect	35	Deleterious	-2.654	Probably damaging	1	0.651641453	Deleterious	23.6
rs74571530	F508C	Effect	59	Deleterious	-6.794	Probably damaging	1	0.641843246	Deleterious	29.5
rs758745885	D513Y	Effect	90	Deleterious	-6.423	Probably damaging	1	0.597220422	Deleterious	28.6
rs368516826	C524R	Effect	87	Deleterious	-10.22	Probably damaging	1	0.569687905	Deleterious	28.3
rs1387755887	G545V	Effect	83	Deleterious	-8.502	Probably damaging	1	0.621163058	Deleterious	28.6
rs1469024267	L548P	Effect	94	Deleterious	-6.609	Probably damaging	1	0.777140505	Deleterious	28.1
rs121908757	S519R	Neutral	-81	Neutral	-1.239	Probably damaging	0.996	0.462454118	Deleterious	28
rs121908755	S519I	Neutral	-16	Deleterious	-3.24	Probably damaging	0.995	0.540770248	Neutral	27.4
rs121909005	S519R	Neutral	-81	Neutral	-1.239	Probably damaging	0.996	0.462454118	Neutral	25.2
rs75527207	G551D	Effect	40	Deleterious	-6.574	Probably damaging	1	0.75222989	Neutral	26.8
rs397508255	R555G	Effect	86	Deleterious	-6.602	Probably damaging	1	0.799480436	Neutral	38
rs75549581	A559S	Effect	89	Deleterious	-2.832	Probably damaging	0.999	0.691602273	Deleterious	27.6
rs397508259	A559E	Effect	97	Deleterious	-4.721	Probably damaging	1	0.757384078	Deleterious	31
rs397508260	R560G	Effect	98	Deleterious	-6.472	Probably damaging	1	0.689609802	Deleterious	49
rs121909006	Y563N	Effect	51	Deleterious	-8.199	Probably damaging	1	0.642969748	Deleterious	29.3
rs397508276	Y569D	Effect	30	Deleterious	-7.558	Probably damaging	1	0.669390533	Deleterious	29.7
rs397508277	Y569C	Effect	2	Deleterious	-6.446	Probably damaging	1	0.669521668	Deleterious	28.7
rs397508282	D572N	Effect	7	Deleterious	-4.655	Probably damaging	0.993	0.727034918	Deleterious	32
rs748393295	D572E	Effect	96	Deleterious	-3.744	Probably damaging	0.993	0.75866299	Deleterious	23.3
rs121908758	P574H	Effect	2	Deleterious	-6.571	Probably damaging	1	0.687942281	Deleterious	31
rs1800100	R668C	Effect	80	Deleterious	-2.577	Probably damaging	1	0.624800084	Deleterious	25.5
rs186089140	S737F	Neutral	-24	Deleterious	-3.438	Probably damaging	1	0.622634051	Deleterious	25.1

rs397508363	R766M	Effect	39	Deleterious	-2.56	Probably damaging	1	0.623460666	Deleterious	27.6
rs1386366130	Q767H	Neutral	-13	Neutral	-1.739	Probably damaging	1	0.62043366	Deleterious	24.7
rs1299482973	S707F	Effect	55	Neutral	-1.796	Probably damaging	0.744	0.585902379	Deleterious	25.8
rs397508375	D806G	Effect	34	Deleterious	-3.365	Probably damaging	1	0.621937441	Deleterious	29.5
rs757165481	Y849H	Effect	64	Deleterious	-3.629	Probably damaging	1	0.618107758	Deleterious	27.9
rs775570582	L165S	Effect	70	Deleterious	-5.076	Probably damaging	1	0.624026793	Deleterious	41
rs1402844924	L165F	Effect	51	Deleterious	-3.384	Probably damaging	1	0.624599327	Deleterious	23.1
rs121909035	H949Y	Effect	9	Deleterious	-5.061	Probably damaging	1	0.72050739	Deleterious	25.7
rs397508444	H949R	Effect	91	Deleterious	-6.732	Probably damaging	1	0.734552388	Deleterious	26.5
rs1191342069	G1241D	Effect	65	Deleterious	-5.962	Probably damaging	1	0.765063796	Deleterious	26
rs397508599	G1244R	Effect	99	Deleterious	-6.814	Probably damaging	1	0.796001161	Deleterious	43
rs267606723	G1244E	Effect	35	Deleterious	-6.815	Probably damaging	1	0.796001161	Deleterious	30
rs397508602	G1249R	Effect	99	Deleterious	-6.813	Probably damaging	1	0.796353604	Deleterious	29.3
rs121909040	G1249E	Effect	30	Deleterious	-6.813	Probably damaging	1	0.796353604	Deleterious	26.9
rs117400534	L1253F	Neutral	-15	Deleterious	-3.256	Probably damaging	1	0.568546906	Deleterious	23.8
rs11971167	D1270Y	Effect	93	Deleterious	-7.661	Probably damaging	1	0.679934439	Deleterious	28.9
rs765549490	D1270G	Effect	91	Deleterious	-5.959	Probably damaging	1	0.542053343	Deleterious	26.5
rs753920616	F508V	Effect	95	Deleterious	-5.778	Probably damaging	1	0.611318672	Deleterious	27.8
rs77010898	W1282C	Effect	76	Deleterious	-2.735	Probably damaging	1	0.537853353	Deleterious	46
rs77902683	R1283M	Effect	30	Deleterious	-5.11	Probably damaging	1	0.712796773	Deleterious	27.7
rs904990724	G1298R	Effect	93	Deleterious	-6.796	Probably damaging	1	0.560994579	Deleterious	48
rs193922522	G1298A	Effect	73	Deleterious	-5.081	Probably damaging	1	0.549625067	Deleterious	33
rs121909042	N1303H	Neutral	-60	Deleterious	-4.262	Probably damaging	1	0.691446673	Deleterious	26.5
rs121909042	N1303Y	Effect	97	Deleterious	-6.819	Probably damaging	1	0.679870663	Deleterious	26.5
rs397508636	N1303I	Effect	97	Deleterious	-7.672	Probably damaging	1	0.657683723	Deleterious	26.6
rs80034486	N1303K	Effect	98	Deleterious	-5.114	Probably damaging	1	0.72911327	Deleterious	23.5
rs201503139	P1306S	Effect	7	Deleterious	-6.819	Probably damaging	1	0.645146816	Deleterious	24.9
rs397508646	D1312G	Effect	43	Deleterious	-5.891	Probably damaging	1	0.61691217	Deleterious	28.2
rs397508653	L1324P	Effect	50	Deleterious	-5.598	Probably damaging	1	0.783795583	Deleterious	29.8
rs755917129	I1267M	Neutral	-80	Neutral	-2.426	Probably damaging	0.31	0.652946028	Deleterious	23.5
rs145545286	L1335F	Effect	61	Deleterious	-3.394	Probably damaging	1	0.615695152	Deleterious	29
rs397508660	L1339F	Effect	7	Neutral	-2.351	Probably damaging	1	0.584324218	Deleterious	26.3
rs544710550	L1339P	Effect	54	Deleterious	-4.351	Probably damaging	1	0.658029142	Deleterious	29.7
rs747324955	G1343S	Effect	57	Deleterious	-5.057	Probably damaging	1	0.558955073	Deleterious	29.6
rs773458471	G1343V	Effect	68	Deleterious	-7.455	Probably damaging	1	0.584477736	Deleterious	27.7
rs1313341594	L1346Q	Effect	84	Deleterious	-4.627	Probably damaging	1	0.764805862	Deleterious	29.5
rs201686600	G1349S	Effect	98	Deleterious	-4.991	Probably damaging	1	0.710090846	Deleterious	31
rs113857788	Q1352H	Effect	73	Deleterious	-4.19	Probably damaging	1	0.694902061	Deleterious	23.7
rs1252048837	L1356S	Effect	34	Deleterious	-4.705	Probably damaging	1	0.6901479	Deleterious	44
rs748223886	R1358T	Effect	83	Deleterious	-4.924	Probably damaging	1	0.702333972	Deleterious	29.9
rs397508670	A1364V	Neutral	-53	Deleterious	-2.678	Probably damaging	1	0.550771818	Deleterious	27.2
rs770345073	I1366F	Effect	49	Deleterious	-3.352	Probably damaging	0.999	0.599990147	Deleterious	28.2
rs200955612	I1366N	Effect	77	Deleterious	-5.759	Probably damaging	1	0.743459658	Deleterious	29.5
rs761271867	I1366M	Effect	39	Neutral	-2.459	Probably damaging	1	0.648275557	Deleterious	23.8
rs767002769	L1369F	Neutral	-19	Deleterious	-3.091	Probably damaging	1	0.554032643	Deleterious	26.5
rs760336091	D1370H	Effect	90	Deleterious	-5.681	Probably damaging	1	0.78358418	Deleterious	30

Note: VaID=Variation ID; E=Effect; N=Neutral; PD=Probably Damage; L=Label; D=Deleterious; C=CADD; S=Score

***Table 3**. Disease association analysis of CFTR nsSNPs using P-Mut, PhD-SNP, SNPs & GO, and Meta-SNP tools.*

VaID	Mutation	P-Mut		PhD-SNP		SNP & GO		Meta SNP	
		Pre	Sc 0.79	Pre	Sc ≥ 6	Pre	Sc	Pre	Sc
rs1031657153	P99A	TRUE	0.7721	Disease	4	Disease	10	Disease	1
rs397508467	P99L	TRUE	0.9279	Disease	6	Disease	10	Disease	5
rs397508490	L102P	TRUE	0.9279	Disease	7	Disease	10	Disease	6
rs397508509	I105N	TRUE	0.9173	Disease	8	Disease	10	Disease	6
rs397508522	Y109N	TRUE	0.7118	Disease	1	Disease	10	Disease	6
rs121909031	Y109C	TRUE	0.7118	Disease	1	Disease	10	Disease	6
rs113993958	D110Y	TRUE	0.5124	Disease	3	Disease	10	Disease	6
rs140502196	P111L	TRUE	0.7213	neutral	3	Disease	10	neutral	0
rs397508551	N113I	TRUE	0.5655	neutral	3	Disease	10	neutral	0
rs761370893	E116G	FALSE	0.4718	neutral	7	Disease	10	neutral	2
rs201958172	A120P	TRUE	0.5839	neutral	6	Disease	10	Disease	3
rs397508592	Y122H	TRUE	0.7219	neutral	4	Disease	10	Disease	3
rs377295859	Y122C	TRUE	0.6933	neutral	4	Disease	10	Disease	5
rs397508609	G126D	TRUE	0.8055	Disease	6	Disease	10	Disease	6
rs1162745955	L129H	TRUE	0.9279	Disease	2	Disease	10	Disease	6
rs397508674	L137H	TRUE	0.8931	Disease	4	Disease	10	Disease	6
rs1800078	L138P	TRUE	0.9279	Disease	3	Disease	10	Disease	6
rs397508718	G149R	TRUE	0.7567	Disease	6	Disease	10	Disease	9
rs397508719	G149E	TRUE	0.8259	Disease	7	Disease	10	Disease	7
rs397508723	A155P	TRUE	0.9239	Disease	7	Disease	10	Disease	8
rs397508724	S158C	TRUE	0.5644	neutral	4	Disease	10	Disease	2
rs397508727	L159S	TRUE	0.5754	neutral	6	Disease	10	Disease	1
rs397508729	Y161D	TRUE	0.9279	Disease	6	Disease	10	Disease	7
rs397508730	Y161S	TRUE	0.9279	Disease	4	Disease	10	Disease	5
rs397508736	L165S	TRUE	0.7567	neutral	1	Disease	10	Disease	3
rs80282562	G178R	TRUE	0.9214	Disease	5	Disease	10	Disease	7
rs397508748	G178E	TRUE	0.9279	Disease	6	Disease	10	Disease	5
rs397508751	L183I	TRUE	0.6737	neutral	5	Disease	10	neutral	0
rs766640075	L188P	TRUE	0.6091	Disease	8	Disease	10	Disease	6
rs397508756	D192N	TRUE	0.5102	neutral	4	Disease	10	Disease	1
rs397508758	D192G	FALSE	0.4395	neutral	6	Disease	10	Disease	2
rs755405930	E193G	TRUE	0.609	neutral	2	Disease	10	Disease	4
rs376008630	G194R	TRUE	0.7822	neutral	6	Disease	10	Disease	6
rs397508765	H199Q	TRUE	0.6365	neutral	5	Disease	10	Disease	3
rs1457675231	F200S	TRUE	0.5613	neutral	6	Disease	10	Disease	1
rs121908803	P205S	TRUE	0.746	neutral	1	Disease	10	Disease	2
rs397508769	P205R	TRUE	0.9279	Disease	5	Disease	10	Disease	7
rs121908752	L206W	TRUE	0.7686	Disease	5	Disease	10	Disease	6
rs1227994401	Q207H	TRUE	0.7654	Disease	7	Disease	10	Disease	5

rs759719664	L180F	TRUE	0.581	neutral	4	Disease	10	Disease	5
rs397508776	W216C	TRUE	0.6975	neutral	4	Disease	10	Disease	6
rs770891254	G226E	TRUE	0.9279	Disease	5	Disease	10	Disease	6
rs397508785	Q237H	TRUE	0.724	Disease	3	Disease	10	Disease	6
rs397508789	G241W	TRUE	0.7215	neutral	0	Disease	10	Disease	6
rs377514639	R258I	TRUE	0.9279	Disease	6	Disease	10	Disease	7
rs1296578005	K273Q	TRUE	0.9279	Disease	6	Disease	10	Disease	4
rs756036343	K273M	TRUE	0.9279	Disease	1	Disease	10	Disease	5
rs397508800	W277R	TRUE	0.9279	Disease	6	Disease	10	Disease	7
rs151073129	I285F	TRUE	0.9239	neutral	3	Disease	10	Disease	0
rs1204521684	V317G	TRUE	0.7371	Disease	0	Disease	10	Disease	5
rs121909011	R334W	TRUE	0.77	Disease	4	Disease	10	Disease	5
rs397508146	L346P	TRUE	0.9279	Disease	7	Disease	10	Disease	6
rs77932196	R347P	TRUE	0.9279	Disease	3	Disease	10	Disease	6
rs397508188	L441P	TRUE	0.9279	Disease	7	Disease	10	Disease	4
rs121908805	S466L	TRUE	0.6073	neutral	3	Disease	10	Disease	2
rs1800089	L467F	FALSE	0.4722	neutral	5	Disease	10	Disease	2
rs139573311	L467P	TRUE	0.9279	Disease	7	Disease	10	Disease	5
rs397508202	L468P	TRUE	0.9279	Disease	6	Disease	10	Disease	5
rs79282516	G480S	TRUE	0.8104	Disease	6	Disease	10	Disease	3
rs397508208	G480D	TRUE	0.8661	Disease	6	Disease	10	Disease	3
rs200626971	W496C	TRUE	0.9279	Disease	7	Disease	10	Disease	6
rs774945680	G500D	TRUE	0.5927	neutral	5	Disease	10	Disease	3
rs397508222	I502N	TRUE	0.9279	Disease	5	Disease	10	Disease	5
rs397508224	I506S	TRUE	0.9279	Disease	7	Disease	10	Disease	5
rs1800092	I506M	TRUE	0.9239	Disease	2	Disease	10	Disease	5
rs74571530	F508C	TRUE	0.7808	Disease	5	Disease	10	Disease	5
rs758745885	D513Y	TRUE	0.8259	Disease	5	Disease	10	Disease	5
rs368516826	C524R	TRUE	0.9279	Disease	8	Disease	10	Disease	6
rs1387755887	G545V	TRUE	0.9279	Disease	8	Disease	10	Disease	9
rs1469024267	L548P	TRUE	0.9279	Disease	6	Disease	10	Disease	5
rs121908757	S519R	FALSE	0.4215	neutral	7	Disease	10	neutral	6
rs121908755	S519I	TRUE	0.514	neutral	5	Disease	10	neutral	4
rs121909005	S519R	TRUE	0.9279	neutral	7	Disease	10	neutral	6
rs75527207	G551D	TRUE	0.9279	Disease	6	Disease	10	Disease	7
rs397508255	R555G	TRUE	0.9279	Disease	6	Disease	10	Disease	7
rs75549581	A559S	TRUE	0.9174	Disease	6	Disease	10	Disease	5
rs397508259	A559E	TRUE	0.9279	Disease	7	Disease	10	Disease	7
rs397508260	R560G	TRUE	0.9279	Disease	6	Disease	10	Disease	7
rs121909006	Y563N	TRUE	0.9279	Disease	6	Disease	10	Disease	3
rs397508276	Y569D	TRUE	0.9279	Disease	7	Disease	10	Disease	5
rs397508277	Y569C	TRUE	0.8259	Disease	6	Disease	10	Disease	5
rs397508282	D572N	TRUE	0.9239	Disease	5	Disease	10	Disease	7
rs748393295	D572E	TRUE	0.9239	Disease	3	Disease	10	Disease	6
rs121908758	P574H	TRUE	0.9279	Disease	7	Disease	10	Disease	5
rs1800100	R668C	TRUE	0.529	Disease	5	Disease	10	Disease	4

rs186089140	S737F	TRUE	0.5851	neutral	4	Disease	10	neutral	3
rs397508363	R766M	TRUE	0.6808	neutral	5	Disease	10	Disease	5
rs1386366130	Q767H	FALSE	0.4504	Disease	2	Disease	10	neutral	4
rs1299482973	S707F	FALSE	0.4427	Disease	1	Disease	10	Disease	1
rs397508375	D806G	TRUE	0.5329	Disease	5	Disease	10	Disease	1
rs757165481	Y849H	TRUE	0.8113	Disease	5	Disease	10	Disease	5
rs775570582	L165S	TRUE	0.7567	neutral	1	Disease	10	Disease	3
rs1402844924	L165F	TRUE	0.6231	neutral	3	Disease	10	Disease	0
rs121909035	H949Y	TRUE	0.6803	neutral	1	Disease	10	Disease	3
rs397508444	H949R	TRUE	0.9239	neutral	1	Disease	10	Disease	6
rs1191342069	G1241D	TRUE	0.9279	Disease	7	Disease	10	Disease	4
rs397508599	G1244R	TRUE	0.9279	Disease	3	Disease	10	Disease	10
rs267606723	G1244E	TRUE	0.9279	Disease	4	Disease	10	Disease	10
rs397508602	G1249R	TRUE	0.9279	Disease	7	Disease	10	Disease	10
rs121909040	G1249E	TRUE	0.9279	Disease	8	Disease	10	Disease	10
rs117400534	L1253F	TRUE	0.6158	Disease	4	Disease	10	neutral	1
rs11971167	D1270Y	TRUE	0.9279	Disease	8	Disease	10	Disease	7
rs765549490	D1270G	TRUE	0.8661	Disease	5	Disease	10	Disease	4
rs753920616	F508V	TRUE	0.8132	Disease	7	Disease	10	Disease	5
rs77010898	W1282C	TRUE	0.7382	Disease	8	Disease	10	Disease	5
rs77902683	R1283M	TRUE	0.9279	Disease	4	Disease	10	Disease	9
rs904990724	G1298R	TRUE	0.9214	Disease	8	Disease	10	Disease	7
rs193922522	G1298A	TRUE	0.7953	neutral	6	Disease	10	neutral	1
rs121909042	N1303H	TRUE	0.9279	Disease	5	Disease	10	Disease	10
rs121909042	N1303Y	TRUE	0.7724	Disease	6	Disease	10	Disease	10
rs397508636	N1303I	TRUE	0.9279	Disease	7	Disease	10	Disease	10
rs80034486	N1303K	TRUE	0.9279	Disease	5	Disease	10	Disease	8
rs201503139	P1306S	TRUE	0.9239	neutral	1	Disease	10	Disease	2
rs397508646	D1312G	TRUE	0.9279	Disease	5	Disease	10	Disease	2
rs397508653	L1324P	TRUE	0.9279	Disease	7	Disease	10	Disease	4
rs755917129	I1267M	TRUE	0.6997	neutral	1	Disease	10	neutral	1
rs145545286	L1335F	TRUE	0.8347	Disease	6	Disease	10	Disease	2
rs397508660	L1339F	TRUE	0.5875	neutral	2	Disease	10	Disease	3
rs544710550	L1339P	TRUE	0.817	Disease	6	Disease	10	Disease	4
rs747324955	G1343S	TRUE	0.8335	Disease	1	Disease	10	Disease	4
rs773458471	G1343V	TRUE	0.9279	Disease	6	Disease	10	Disease	5
rs1313341594	L1346Q	TRUE	0.9279	Disease	4	Disease	10	Disease	5
rs201686600	G1349S	TRUE	0.9239	Disease	4	Disease	10	Disease	8
rs113857788	Q1352H	TRUE	0.9239	Disease	6	Disease	10	Disease	5
rs1252048837	L1356S	TRUE	0.9279	Disease	1	Disease	10	Disease	2
rs748223886	R1358T	TRUE	0.9279	Disease	3	Disease	10	Disease	10
rs397508670	A1364V	TRUE	0.7081	neutral	1	Disease	10	Disease	0
rs770345073	I1366F	TRUE	0.7909	Disease	3	Disease	10	Disease	1
rs200955612	I1366N	TRUE	0.9279	Disease	5	Disease	10	Disease	3
rs761271867	I1366M	TRUE	0.9174	neutral	6	Disease	10	Disease	3
rs767002769	L1369F	TRUE	0.7029	neutral	4	Disease	10	Disease	2

rs760336091	D1370H	TRUE	0.9279	neutral	2	Disease	10	Disease	10

Note: VaID=Variation ID; Pre=Prediction

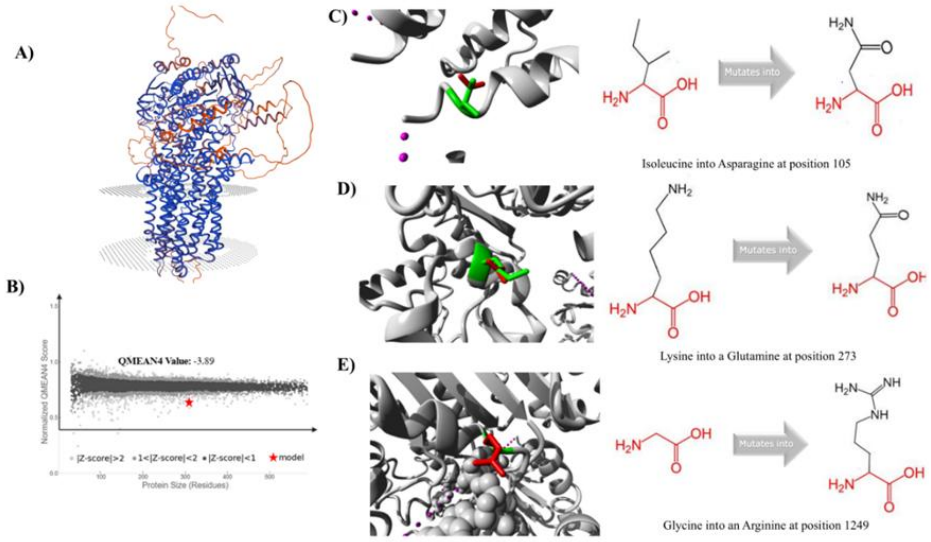

Figure 4. *Structural modeling and mutational analysis of the CFTR protein. (A) Homology-modeled structure of the CFTR protein. (B) QMEAN validation plot. (C) Structural representation of the I105N mutation. (D) Structural representation of the K273Q mutation. (E) Structural representation of the G1249R mutation.*

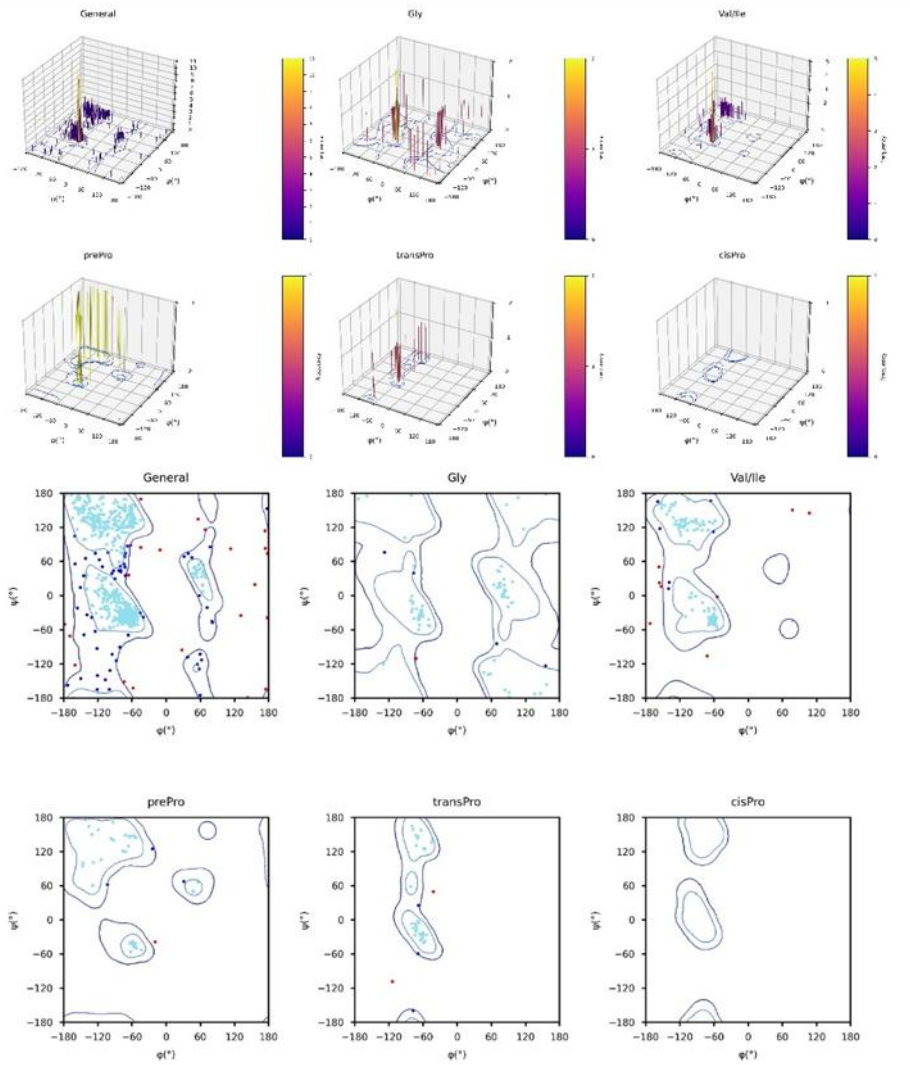

Figure 5. *2D and 3D Ramachandran plots validating the stereochemical quality of the modeled CFTR structure.*

Variant effect on protein stability

In *Figure 6*, a total of 132 nsSNPs were submitted to i-Mutant 3.0 for RI prediction, revealing that 21 nsSNPs increase protein stability, including P99L, K273M, L441P, G545V, S707F, G178E, N113I, A120P, G226E, S519R, S519I, G1249E, G1249R, I1366I, and so on. Additionally, MUPro analysis indicated that P99L, K273M, L441P, G545V, and S707F enhance CFTR stability. As summarized in *Table 4*, i-Stable predicted that 26 nsSNPs increase protein stability, whereas 106 missense variants lead to decreased stability, highlighting the overall destabilizing impact of most CFTR mutations.

Table 4*. Protein stability analysis of CFTR variants using MuPro, I-Mutant, and iStable tools.*

Variation ID	Mutation	Mu Pro		i-mutant		i-stable	
		Prediction	Detal delta ≥ 0.5	Stability	RI	Prediction	Score ≥ 0.6
rs1031657153	P99A	DECREASE stability	-0.5557076	Decrease	9	Decrease	0.800281
rs397508467	P99L	INCREASE	0.6099566	Decrease	6	Decrease	0.798063

rs397508490	L102P	DECREASE stability	-1.5990922	Decrease	6	Decrease	0.801118
rs397508509	I105N	DECREASE stability	-1.9706942	Decrease	8	Decrease	0.830344
rs397508522	Y109N	DECREASE stability	-1.5829391	Decrease	8	Decrease	0.651673
rs121909031	Y109C	DECREASE stability	-1.4308958	Decrease	4	Decrease	0.701401
rs113993958	D110Y	DECREASE stability	-0.6992614	Decrease	0	Decrease	0.788
rs140502196	P111L	DECREASE stability	-0.7306786	Decrease	2	Decrease	0.746703
rs397508551	N113I	DECREASE stability	-0.648336	Increase	5	Increase	0.505217
rs761370893	E116G	DECREASE stability	-1.6066962	Decrease	6	Decrease	0.914007
rs201958172	A120P	DECREASE stability	-1.1242569	Increase	5	Increase	0.79477
rs397508592	Y122H	DECREASE stability	-1.7476217	Decrease	7	Decrease	0.801822
rs377295859	Y122C	DECREASE stability	-1.4771859	Decrease	5	Decrease	0.788527
rs397508609	G126D	DECREASE stability	-0.3152133	Decrease	6	Increase	0.656059
rs1162745955	L129H	DECREASE stability	-1.7093343	Decrease	8	Decrease	0.830763
rs397508674	L137H	DECREASE stability	-1.7937677	Decrease	8	Decrease	0.788962
rs1800078	L138P	DECREASE stability	-1.7996118	Decrease	3	Decrease	0.828728
rs397508718	G149R	DECREASE stability	-0.7848849	Decrease	0	Decrease	0.70064
rs397508719	G149E	DECREASE stability	-0.6846736	Decrease	1	Decrease	0.720955
rs397508723	A155P	DECREASE stability	-1.4022757	Increase	2	Increase	0.745779
rs397508724	S158C	DECREASE stability	-0.5678241	Decrease	2	Decrease	0.768076
rs397508727	L159S	DECREASE stability	-1.7831079	Decrease	9	Decrease	0.826367
rs397508729	Y161D	DECREASE stability	-1.6065272	Increase	2	Decrease	0.681074
rs397508730	Y161S	DECREASE stability	-2.0958528	Decrease	4	Decrease	0.88616
rs397508736	L165S	DECREASE stability	-2.5088231	Decrease	8	Decrease	0.896556
rs80282562	G178R	DECREASE stability	-1.1880191	Decrease	4	Increase	0.554817
rs397508748	G178E	DECREASE stability	-1.1226603	Increase	0	Increase	0.786076
rs397508751	L183I	DECREASE stability	-0.78709659	Decrease	7	Decrease	0.62128
rs766640075	L188P	DECREASE stability	-2.6840999	Decrease	3	Decrease	0.826112
rs397508756	D192N	DECREASE stability	-0.548786	Decrease	7	Decrease	0.777595
rs397508758	D192G	DECREASE stability	-1.2490357	Decrease	7	Decrease	0.851055
rs755405930	E193G	DECREASE stability	-1.2823724	Decrease	7	Decrease	0.530562
rs376008630	G194R	DECREASE stability	-0.41320231	Decrease	4	Decrease	0.719897
rs397508765	H199Q	DECREASE stability	-0.9776213	Decrease	4	Decrease	0.676365
rs1457675231	F200S	DECREASE stability	-1.5427317	Decrease	9	Decrease	0.807525
rs121908803	P205S	DECREASE stability	-1.2797582	Decrease	8	Decrease	0.770298
rs397508769	P205R	DECREASE stability	-1.1320674	Decrease	5	Decrease	0.742026
rs121908752	L206W	DECREASE stability	-1.0927885	Decrease	5	Decrease	0.871222

rs1227994401	Q207H	DECREASE stability	-0.814767	Decrease	8	Decrease	0.768691
rs759719664	L180F	DECREASE stability	-0.7117823	Decrease	4	Decrease	0.819394
rs397508776	W216C	DECREASE stability	-0.6594687	Decrease	7	Decrease	0.822703
rs770891254	G226E	DECREASE stability	-0.2546524	increase	4	Decrease	0.515619
rs397508785	Q237H	DECREASE stability	-0.63513713	Decrease	9	Decrease	0.598594
rs397508789	G241W	DECREASE stability	-0.3556606	increase	2	Increase	0.796031
rs377514639	R258I	DECREASE stability	-0.6400463	Decrease	4	Decrease	0.793303
rs1296578005	K273Q	DECREASE stability	-0.3246713	Decrease	6	Decrease	0.756817
rs756036343	K273M	INCREASE stability	0.1555522	Decrease	2	Increase	0.639595
rs397508800	W277R	DECREASE stability	-0.4583815	Decrease	7	Increase	0.679151
rs151073129	I285F	DECREASE stability	-0.82942098	Decrease	3	Decrease	0.872513
rs1204521684	V317G	DECREASE stability	-2.0775997	Decrease	10	Decrease	0.827884
rs121909011	R334W	DECREASE stability	-1.1541102	Decrease	2	Decrease	0.757645
rs397508146	L346P	DECREASE stability	-1.6409523	Decrease	6	Decrease	0.893797
rs77932196	R347P	DECREASE stability	-1.2978301	Decrease	3	Decrease	0.750586
rs397508188	L441P	DECREASE stability	-1.9945794	Decrease	8	Decrease	0.82827
rs121908805	S466L	INCREASE stability	0.3877408	Increase	3	Increase	0.753838
rs1800089	L467F	DECREASE stability	-1.2328324	Decrease	6	Decrease	0.86033
rs139573311	L467P	DECREASE stability	-1.9143963	Decrease	5	Decrease	0.851713
rs397508202	L468P	DECREASE stability	-2.1603347	Decrease	5	Decrease	0.833299
rs79282516	G480S	DECREASE stability	-1.1809141	Decrease	5	Decrease	0.810659
rs397508208	G480D	DECREASE stability	-0.9116127	Decrease	5	Decrease	0.792936
rs200626971	W496C	DECREASE stability	-0.9124014	Decrease	8	Decrease	0.812659
rs774945680	G500D	DECREASE stability	-0.3619342	Decrease	7	Increase	0.603067
rs397508222	I502N	DECREASE stability	-1.2472223	Decrease	7	Decrease	0.555645
rs397508224	I506S	DECREASE stability	-1.9224014	Decrease	9	Decrease	0.878466
rs1800092	I506M	DECREASE stability	-1.1512498	Decrease	9	Decrease	0.853986
rs74571530	F508C	DECREASE stability	-1.4364461	Decrease	7	Decrease	0.824526
rs758745885	D513Y	DECREASE stability	-0.2967828	Decrease	3	Increase	0.615206
rs368516826	C524R	DECREASE stability	-1.3820722	Decrease	3	Decrease	0.782475
rs1387755887	G545V	INCREASE stability	0.3815065	Decrease	5	Decrease	0.777367
rs1469024267	L548P	DECREASE stability	-2.1186779	Decrease	4	Decrease	0.835041
rs121908757	S519R	DECREASE stability	-1.3823772	Increase	1	Increase	0.703129
rs121908755	S519I	DECREASE stability	-0.9041675	Decrease	0	Increase	0.755216
rs121909005	S519R	DECREASE stability	-1.3823772	Increase	1	Increase	0.703129
rs75527207	G551D	DECREASE stability	-0.6971572	Decrease	2	Decrease	0.7189
rs397508255	R555G	DECREASE	-1.8597025	Decrease	7	Decrease	0.816327

		stability					
rs75549581	A559S	DECREASE stability	-1.0994891	Decrease	9	Decrease	0.864647
rs397508259	A559E	DECREASE stability	-0.8854481	Decrease	7	Decrease	0.511478
rs397508260	R560G	DECREASE stability	-1.8293962	Decrease	7	Decrease	0.829416
rs121909006	Y563N	DECREASE stability	-1.2866212	Decrease	5	Decrease	0.788303
rs397508276	Y569D	DECREASE stability	-1.6791017	Decrease	6	Decrease	0.761464
rs397508277	Y569C	DECREASE stability	-1.4916056	Decrease	6	Decrease	0.777235
rs397508282	D572N	DECREASE stability	-0.7668229	Decrease	7	Decrease	0.577362
rs748393295	D572E	DECREASE stability	-0.41672522	Decrease	1	Increase	0.641062
rs121908758	P574H	DECREASE stability	-1.707245	Decrease	8	Decrease	0.807257
rs1800100	R668C	DECREASE stability	-0.743323	Decrease	3	Decrease	0.794376
rs186089140	S737F	DECREASE stability	-0.6939322	increase	6	Decrease	0.508201
rs397508363	R766M	DECREASE stability	-0.4649359	Decrease	5	Increase	0.595122
rs1386366130	Q767H	DECREASE stability	-1.1677499	Decrease	7	Decrease	0.736198
rs1299482973	S707F	INCREASE stability	0.3493291	increase	1	Increase	0.809512
rs397508375	D806G	DECREASE stability	-1.4655821	Decrease	2	Decrease	0.797931
rs757165481	Y849H	DECREASE stability	-1.4566337	Decrease	2	Decrease	0.84272
rs775570582	L165S	DECREASE stability	-2.5088231	Decrease	8	Decrease	0.896556
rs1402844924	L165F	DECREASE stability	-1.5734354	Decrease	3	Decrease	0.892523
rs121909035	H949Y	DECREASE stability	-0.680929	increase	7	Increase	0.523866
rs397508444	H949R	DECREASE stability	-0.7707563	Decrease	1	Decrease	0.756359
rs1191342069	G1241D	DECREASE stability	-0.8034987	increase	1	Increase	0.729624
rs397508599	G1244R	DECREASE stability	-0.6867931	increase	0	Decrease	0.57188
rs267606723	G1244E	DECREASE stability	-0.5285789	increase	7	Decrease	0.558142
rs397508602	G1249R	DECREASE stability	-0.6374709	Decrease	0	Increase	0.739014
rs121909040	G1249E	DECREASE stability	-0.4102457	increase	7	Increase	0.754535
rs117400534	L1253F	DECREASE stability	-1.0673433	Decrease	7	Decrease	0.867705
rs11971167	D1270Y	DECREASE stability	-0.9460165	increase	4	Decrease	0.513168
rs765549490	D1270G	DECREASE stability	-1.7353752	Decrease	1	Decrease	0.803916
rs753920616	F508V	DECREASE stability	-1.360253	Decrease	8	Decrease	0.842255
rs77010898	W1282C	DECREASE stability	-0.6226598	Decrease	8	Decrease	0.879048
rs77902683	R1283M	DECREASE stability	-0.3487679	Decrease	6	Increase	0.588298
rs904990724	G1298R	DECREASE stability	-0.3476638	Decrease	7	Increase	0.623493
rs193922522	G1298A	DECREASE stability	-0.59709621	Decrease	8	Decrease	0.77595
rs121909042	N1303H	DECREASE stability	-1.0868868	Decrease	9	Decrease	0.767533
rs121909042	N1303Y	DECREASE stability	-0.50017672	Decrease	1	Decrease	0.73393
rs397508636	N1303I	DECREASE stability	-0.19755439	increase	4	Increase	0.559203

rs80034486	N1303K	DECREASE stability	-1.0937566	Decrease	6	Decrease	0.750646
rs201503139	P1306S	DECREASE stability	-0.9820391	Decrease	8	Decrease	0.820418
rs397508646	D1312G	DECREASE stability	-1.404051	increase	6	Decrease	0.513825
rs397508653	L1324P	DECREASE stability	-1.9579279	Decrease	7	Decrease	0.876623
rs755917129	I1267M	DECREASE stability	-1.0247056	Decrease	8	Increase	0.607692
rs145545286	L1335F	DECREASE stability	-1.2160428	Decrease	6	Decrease	0.887374
rs397508660	L1339F	DECREASE stability	-1.1785594	Decrease	4	Decrease	0.849935
rs544710550	L1339P	DECREASE stability	-2.1528361	Decrease	5	Decrease	0.853875
rs747324955	G1343S	DECREASE stability	-0.9196335	Decrease	6	Decrease	0.676292
rs773458471	G1343V	DECREASE stability	-0.3173998	Decrease	4	Decrease	0.628187
rs1313341594	L1346Q	DECREASE stability	-1.334338	Decrease	7	Decrease	0.85213
rs201686600	G1349S	DECREASE stability	-1.1678918	Decrease	5	Decrease	0.863195
rs113857788	Q1352H	DECREASE stability	-0.478542	Decrease	7	Decrease	0.86203
rs1252048837	L1356S	DECREASE stability	-1.9304028	Decrease	8	Decrease	0.832741
rs748223886	R1358T	DECREASE stability	-1.2758966	Decrease	4	Decrease	0.812788
rs397508670	A1364V	DECREASE stability	-1.1830918	increase	5	Decrease	0.620044
rs770345073	I1366F	DECREASE stability	-1.1200946	Decrease	6	Decrease	0.892195
rs200955612	I1366N	DECREASE stability	-1.6891954	Decrease	4	Decrease	0.869505
rs761271867	I1366M	DECREASE stability	-0.93357778	Decrease	7	Decrease	0.875433
rs767002769	L1369F	DECREASE stability	-1.2780019	Decrease	3	Decrease	0.807223
rs760336091	D1370H	DECREASE stability	-1.2839117	Decrease	5	Decrease	0.695465

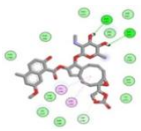
CFTR+Chromophore

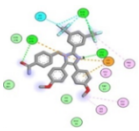
CFTR+Apoptozole

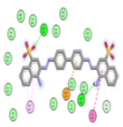
CFTR+Congo red

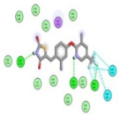
CFTR+Cpd-β

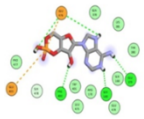
CFTR+cAMP

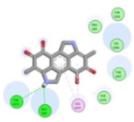
CFTR+ Melanin

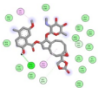
G1249R + Chromophore


G1249R + Apoptozole

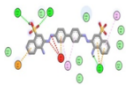
G1249R + Congo red


G1249R + Melanin

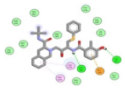
G1249R + Nelfinavir


G1249R + NAD


I105N+ Apoptozole


I105N+ cAMP


I105N+ Chromophore


I105N+ Congo red

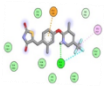
I105N+ Cpd-β


I105N+ NAD


K273Q+ Apoptozole

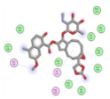
K273Q+ Chromophore

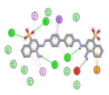
K273Q+ Congo red


K273Q+ Melanin


K273Q+ NAD

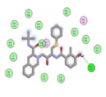
K273Q+ Nelfinavir

Figure 6. *Visualization of ligand interactions with native CFTR and its variants (I105N, K273Q, and G1249R) using Discovery Studio Visualizer.*

Evolutionary conservation and PTM analysis

A total of 132 nsSNPs in the CFTR gene were examined to evaluate their evolutionary conservation and possible post-translational modifications (PTMs). Analysis with CONSURF showed that most variants are located in highly conserved regions, with scores ranging from 1 to 9 (*Table 5*). Of these, 98 nsSNPs had scores between 7 and 9, suggesting important roles in protein structure or function, and 46 variants scored the maximum of 9, indicating residues that are highly conserved and likely critical for protein activity. PTM analysis using Musite Deep predicted three sites of potential modification such as C524 as an S-palmitoyl cysteine, and S707 and S737 as phosphoserine residues. These sites may play regulatory roles affecting the stability and function of the CFTR protein. Combining the information from conservation and PTM analyses allows identification of nsSNPs with the highest potential to disrupt protein function, which can be prioritized for further structural and functional studies. Our analysis identified 30 nsSNPs in the CFTR gene as highly deleterious, based on consistent predictions across 15 computational algorithms, that were subsequently prioritized for molecular modeling and structural studies to evaluate their potential impact on CFTR protein dynamics.

Table 5*. Identification of evolutionary conservation of nsSNPs in the CFTR gene.*

VaID	Mut	CS	VaID	Mut	CS	VaID	Mut	CS
rs1031657153	P99A	9,e,f	rs377514639	R258I	9,e,f	rs1299482973	S707F	7,e
rs397508467	P99L	9,e,f	rs1296578005	K273Q	9,e,f	rs397508375	D806G	9,b,s
rs397508490	L102P	8,b	rs756036343	K273M	9,e,f	rs757165481	Y849H	9,e,f
rs397508509	I105N	9,b,s	rs397508800	W277R	9,b,s	rs775570582	L165S	8,b
rs397508522	Y109N	7,b	rs151073129	I285F	8,b	rs1402844924	L165F	8,b
rs121909031	Y109C	7,b	rs1204521684	V317G	6,b	rs121909035	H949Y	5,e
rs113993958	D110Y	5,e	rs121909011	R334W	7,e	rs397508444	H949R	5,e
rs140502196	P111L	1,e	rs397508146	L346P	6,b	rs1191342069	G1241D	8,b
rs397508551	N113I	4,e	rs77932196	R347P	9,e,f	rs397508599	G1244R	9,b,s
rs761370893	E116G	6,e	rs397508188	L441P	9,e,f	rs267606723	G1244E	9,b,s
rs201958172	A120P	7,b	rs121908805	S466L	8,b	rs397508602	G1249R	9,e,f
rs397508592	Y122H	1,b	rs1800089	L467F	8,b	rs121909040	G1249E	9,e,f
rs377295859	Y122C	1,b	rs139573311	L467P	8,b	rs117400534	L1253F	7,b
rs397508609	G126D	7,b	rs397508202	L468P	6,b	rs11971167	D1270Y	8,e,f
rs1162745955	L129H	4,b	rs79282516	G480S	8,e,f	rs765549490	D1270G	8,e,f
rs397508674	L137H	4,b	rs397508208	G480D	8,e,f	rs753920616	F508V	7,b
rs1800078	L138P	4,b	rs200626971	W496C	6,b	rs77010898	W1282C	8,b
rs397508718	G149R	8,b	rs774945680	G500D	3,b	rs77902683	R1283M	9,e,f
rs397508719	G149E	8,b	rs397508222	I502N	7,b	rs904990724	G1298R	5,b
rs397508723	A155P	9,b,s	rs397508224	I506S	9,b,s	rs193922522	G1298A	5,b
rs397508724	S158C	9,b,s	rs1800092	I506M	9,b,s	rs121909042	N1303H	9,e,f
rs397508727	L159S	8,b	rs74571530	F508C	7,b	rs121909042	N1303Y	9,e,f
rs397508729	Y161D	9,b,s	rs758745885	D513Y	4,e	rs397508636	N1303I	9,e,f
rs397508730	Y161S	9,b,s	rs368516826	C524R	8,b	rs80034486	N1303K	9,e,f
rs397508736	L165S	8,b	rs1387755887	G545V	9,b,s	rs201503139	P1306S	7,e
rs80282562	G178R	7,e	rs1469024267	L548P	9,b,s	rs397508646	D1312G	5,e
rs397508748	G178E	7,e	rs121908757	S519R	1,e	rs397508653	L1324P	7,b
rs397508751	L183I	9,b,s	rs121908755	S519I	1,e	rs755917129	I1267M	8,b
rs766640075	L188P	8,b	rs121909005	S519R	1,e	rs145545286	L1335F	7,b
rs397508756	D192N	9,e,f	rs75527207	G551D	9,e,f	rs397508660	L1339F	6,e
rs397508758	D192G	9,e,f	rs397508255	R555G	9,e,f	rs544710550	L1339P	6,e
rs755405930	E193G	3,e	rs75549581	A559S	9,b,s	rs747324955	G1343S	8,e,f
rs376008630	G194R	5,e	rs397508259	A559E	9,b,s	rs773458471	G1343V	8,e,f
rs397508765	H199Q	9,b,s	rs397508260	R560G	9,e,f	rs1313341594	L1346Q	7,b
rs1457675231	F200S	4b	rs121909006	Y563N	8,b	rs201686600	G1349S	9,e,f
rs121908803	P205S	9,b,s	rs397508276	Y569D	6,b	rs113857788	Q1352H	9,e,f
rs397508769	P205R	9,b,s	rs397508277	Y569C	6,b	rs1252048837	L1356S	8,b
rs121908752	L206W	6,b	rs397508282	D572N	9,e,f	rs748223886	R1358T	9,e,f

rs1227994401	Q207H	8,e,f	rs748393295	D572E	9,e,f	rs397508670	A1364V	6,b
rs759719664	L180F	6,b	rs121908758	P574H	8,e,f	rs770345073	I1366F	8,b
rs397508776	W216C	5,b	rs1800100	R668C	9,e,f	rs200955612	I1366N	8,b
rs770891254	G226E	7,b	rs186089140	S737F	9,e,f	rs761271867	I1366M	8,b
rs397508785	Q237H	9,e,f	rs397508363	R766M	9,e,f	rs767002769	L1369F	8,b
rs397508789	G241W	6,e	rs1386366130	Q767H	9,e,f	rs760336091	D1370H	9,e,f

Note: VaID=Variation ID; Mut=Mutation; CS=ConSURF Score.

Modeling and structure validation

The 3D structure of CFTR was generated using SWISS-MODEL with Q2IBA1.1.A (CFTR_CHLAE) as the template. The selected template showed 98.31% sequence identity with the query sequence and yielded a GMQE score of 0.76, indicating a reliable monomeric model. The refined structure, processed through ModRefiner, was validated using the SAVES server suite. ProCheck analysis demonstrated 88.10% of residues in the core regions, with an additional 8.10% in allowed regions, giving 96.2% of residues in favorable conformations overall. ERRAT analysis reported a quality factor of 97.524, while Verify3D confirmed that 52.39% of residues had an acceptable 3D–1D score. The model achieved a QMEAN4 score of –3.29, placing it within the range expected for high-quality structures of comparable size. The red star in the QMEAN plot denoted the global quality estimate, positioned within the favorable region, while the red-shaded area represented the most reliable quality zone. Moreover, TM-align analysis revealed that I105N, K273Q and G1249R exhibited the highest RMSD values (0.93, 0.98, and 0.93 Å, respectively) and were selected for further molecular docking to evaluate potential structural alterations (*Table 6*). *Table 7* summarizes the amino acid substitutions in the CFTR protein, their structural location, size differences, physicochemical changes, and the predicted impact on protein stability and function as assessed using the HOPE server. The stereochemical quality of the modeled CFTR structure was assessed using 2D and 3D Ramachandran plots across (a) general residues (Ala and the remaining 15 amino acids), (b) Gly, (c) Val/Ile, (d) pre-Pro, (e) trans-Pro, and (f) cis-Pro. In the 2D plots, torsion angles in favored, allowed, and disallowed regions were represented by cyan, blue, and red markers, respectively. Glycine residues were denoted by triangles, while all other residues were shown as dots. The 3D plots further illustrated the distribution of torsion angles by vertical bars, providing a quantitative overview of conformational preferences.

***Table 6**. Structural validation of wild-type and mutant protein models using SAVES v6.1 and TM-align.*

rs ID	ERRAT	ProCheck				Verify 3D	TM Align	
	Score	Core	Allow	Generously	Disallowed	Score	RMSD	TM score
Q2IBA1.1.A	97.524	88.10%	8.10%	1.50%	1.80%	52.39%	-	-
A559E	81.0252	88.50%	9.50%	1.00%	1.00%	8.37%	0.89	0.99467
A559S	79.495	88.90%	8.90%	1.20%	1.00%	8.87%	0.85	0.99562
C524R	79.6507	89.20%	8.30%	1.60%	0.90%	9.01%	0.82	0.99553
G480D	82.7454	88.30%	9.30%	1.30%	1.10%	9.30%	0.79	0.99576
G480S	79.7864	88.70%	9.00%	1.60%	0.60%	9.16%	0.69	0.99682
G545V	80.6279	88.40%	8.80%	1.70%	1.10%	8.51%	0.89	0.99544
G1249R	80.6748	88.50%	9.20%	1.30%	1.10%	8.44%	0.93	0.99497
K273Q	83.8258	88.10%	9.50%	1.60%	0.80%	8.37%	0.93	0.99491
L102P	81	89.40%	8.10%	1.60%	0.90%	9.08%	0.85	0.99262
P99L	82.479	88.50%	9.40%	1.10%	0.90%	9.37%	0.76	0.9961
P205R	79.3025	88.90%	8.60%	1.60%	0.90%	10.59%	0.92	0.99488
W496C	82.1705	88.50%	9.30%	1.20%	1.00%	9.23%	0.67	0.99698
Y161D	81.5159	88.50%	9.80%	1.10%	0.60%	9.08%	0.69	0.99672
Y161S	81.8462	89.10%	8.20%	1.60%	1.00%	8.66%	0.62	0.99736
P574H	82.7586	88.20%	9.70%	1.20%	0.90%	8.94%	0.72	0.99652
R258I	81.6031	89.30%	8.60%	1.30%	0.80%	8.51%	0.79	0.99595
W277R	82.5348	88.80%	8.80%	1.40%	1.00%	8.80%	0.71	0.99658
R560G	82.1705	88.50%	9.40%	1.20%	0.90%	9.51%	0.67	0.99695
L1324P	82.1835	88.40%	9.30%	1.10%	1.20%	9.23%	0.76	0.99612
N1303Y	81.0146	88.50%	9.10%	1.00%	1.30%	9.59%	0.74	0.99637
R555G	80.784	88.40%	9.30%	1.40%	0.90%	8.80%	0.8	0.99605
L468P	76.9406	87.80%	9.90%	1.40%	0.90%	9.66%	0.63	0.99733
L548P	80.8623	88.40%	9.80%	1.10%	0.70%	9.44%	0.61	0.99746
I105N	81.4043	88.40%	9.20%	1.60%	0.90%	10.09%	0.98	0.99449
I506S	82.2119	87.90%	10.20%	1.10%	0.80%	8.44%	0.84	0.99486
G149E	80.1836	89.10%	8.80%	1.00%	1.10%	8.80%	0.65	0.9971
L441P	81.6577	89.20%	8.60%	1.10%	1.10%	9.44%	0.9	0.99489
L467P	82.2941	89.00%	8.70%	1.20%	1.10%	8.94%	0.7	0.99672
D1370H	80.9451	88.80%	9.00%	1.20%	1.00%	9.44%	0.73	0.99647
F508V	82.7957	88.90%	9.00%	1.30%	0.90%	9.01%	0.63	0.99732

Table 7*. Structural and functional consequences of CFTR missense variants predicted by HOPE analysis.*

rsID	A.A Change	Mutant Size	Effect on Protein	Variant Location	Amino Acid Properties
rs397508602	G1249R	Larger than wild-type	Disrupts ATP binding, destabilizes domain folding, and interferes with inter-domain communication	ATP-binding site	WT Gly: small, neutral, flexible; Mutant Arg: large, positively charged, less hydrophobic
rs1296578005	K273Q	Smaller than wild-type	Loss of H-bond with Ala959; disrupts salt bridges with Glu278 & Glu1172; destabilizes folding & interactions	Transmembrane domain	WT Lys: large, positively charged, hydrophilic; Mutant Gln: smaller, neutral, polar
rs397508509	I105N	Larger than wild-type	Introduces polar residue into hydrophobic core; disrupts packing; may abolish local folding & domain interactions	Transmembrane domain	WT Ile: small, hydrophobic, buried; Mutant Asn: larger, polar, less hydrophobic

Computational docking of Wild-Type and mutant CFTR proteins

The molecular docking analysis demonstrated that all 25 ligands exhibited binding free energies lower than –4 kcal/mol when docked against the CFTR wild-type protein and I105N, K273Q, and G1249R variants. As shown in *Table 8*, the ligands with the most significant docking scores with Wild and mutant included Apoptozole, chromophore, Congo red, cpd β, cAMP, NAD, Nelfinavir, and melanin. The overall binding patterns were consistent with the known or predicted biological activities of these compounds. Moreover, chromophore (–9.1 kcal/mol with wild-type, –8.7 kcal/mol with K273Q, and –8.5 kcal/mol with G1249R) and apoptozole (–9.0, –8.5, –8.4 kcal/mol, respectively) showed the highest docking score, suggesting a potential to stabilize CFTR structures. Congo Red also demonstrated a high score across all variants, with scores ranging from –8.3 to –8.6 kcal/mol. Additionally, docking analysis revealed that antiviral agents like amprenavir and nelfinavir (–6.2 to –7.8 kcal/mol) and small molecules such as cAMP (–7.0 to –8.0 kcal/mol) interact strongly with CFTR, consistent with their roles in protein folding and CFTR activation. Phenothiazine, chlorpromazine, and natural metabolites, including NAD, biotin, hyaluronic acid, and melanin, showed moderate to strong affinities (–5.1 to –8.7 kcal/mol), suggesting potential effects on CFTR gating, stability, and cellular function. *Table 9* details interacting residues, while 2D Linteraction patterns highlight hydrogen bonds and hydrophobic contacts across wild-type and mutant CFTR, supporting opportunities for drug repurposing and novel CFTR modulators. Apoptozole interacted strongly with wild-type CFTR through multiple hydrogen bonds involving GLN376, LEU375, GLU379, GLN378, LYS381, LYS166, TRP57, and GLU54, with hydrophobic associations contributed by LYS377, LEU61, PRO67, LEU159, and LYS162. In the G1249R mutant, apoptozole established hydrogen bonds with LEU1279, ARG1259, THR1278, LEU1187, ALA959, SER955, THR1176, GLU279, and GLN1280, and hydrophobic contacts with ILE1277, GLN1186, GLY1185, GLN958, PRO1175, PRO960, GLU278, and LEU957. In I105N, it formed hydrogen bonds with GLU402, SER431, GLY437, ASP173, PHE430, SER176, and LEU428, while hydrophobic interactions involved ARG170, LEU436, PHE405, SER431, TRP401, and LYS174. For K273Q, apoptozole bound via hydrogen bonds with GLN1280, ASP1275, THR1278, GLU278, GLN158, ALA959, THR1176, PRO960, ASN1262, LEU1261, LYS1177,

ARG1259, and MET96, in addition to hydrophobic associations with TRP1274, ILE1277, and PRO1175 (*Table 9*).

***Table 8**. PyRx-based molecular docking of ligands with CFTR wild-type and mutant variants.*

Ligands	CFTR Wild	I105N	K273Q	G1249R	Ligands	CFTR Wild	I105N	K273Q	G1249R
Amprenavir	-6.9	-5.8	-6.2	-6.8	Memantine	-5.5	-5.5	-6	-4.9
Apoptozole	-9	-7.9	-8.5	-8.4	NAD	-6.9	-7.2	-8	-7.9
Biotin	-5.6	-5.9	-5.1	-5.1	Nelfinavir	-6.9	-7.1	-7.7	-7.8
cAMP	-7.3	-8	-7	-6.6	Phenothiazine	-6.3	-6	-6.4	-6.3
Chlorpromazine	-5.9	-5.3	-5.7	-5.3	3h-Indole-5,6 Diol	-5.3	-4.7	-6	-5.3
Chlortetracycline	-6.1	-6.3	-6.9	-7.1	3 ID	-6.4	-5	-5.9	-4.9
Chromophore	-9.1	-7.5	-8.7	-8.5	Alpha D-Fucopyranose	-5	-5.3	-4.9	-4.6
Congo Red	-8.6	-8.4	-8.3	-8.5	GLC	-5.5	-5.5	-4.9	-4.5
Cpd B	-7.9	-7.9	-7.5	-7.8	M2P	-6.2	-4.6	-4.7	-4.3
Florbetaben	-6.2	-5.7	-6	-5.4	TVY	-6.6	-6.3	-6	-5.5
GAG	-4.2	-4.6	-4.2	-3.9	Z8T	-5.3	-5.6	-4.6	-4.8
Hyaluronic Acid	-6.1	-6.5	-6.2	-6.1	Z9N	-4.2	-5.3	-4.3	-4.1
Melanin	-7.3	6.6	-7.8	-8.7	-	-	-	-	-

***Table 9**. Interacting residues obtained from docking. CFTR and G1249R, I105N, and K273Q mutant protein structures with ligands show interaction residues and hydrophobic associations.*

Receptor-Ligands	Hydrophilic bonded interactions	Hydrophobic bonded interactions
CFTR+ Apoptozole	GLN376, LEU375, GLU379, GLN378, LYS381, LYS166, TRP57, GLU54	LYS377, GLN376, LEU61, PRO67, LEU159, LYS162
CFTR+ Chromophore	ASN1262, SER962, LEU1260, ASP1275, ILE1277, TRP1274, ASN1274, ASN1184, LYS1177, THR1278, GLU1280, GLN258, GLU1221, MET961	LEU1279, ARG1259
CFTR+ Congo Red	ARG1259, LEU1260, LEU1279, TRP1274, SER1276, ASN1184, THR1278, ILE`177, LYS1177, SER962, GLU1221, ASN1262, LEU1261, MET961, GLN1186	LEU1187, PRO96
CFTR+ Cpd-β	SER1188, THR1278, THR1263, ASN1184, SER1276, ILE1222, TRP1224, LEU1260, SER962, LEU1961	LEU1229, ARG1259, MET961, PRO960, ASN1262, LEU1229
CFTR+ cAMP	GLN378, LYS181, TYR380, SER168, GLU474, ARG170, LEU475, TRP401, SER478, PRO477	GLU476, GLU403
CFTR+ Melanin	TYR1073, GLU504, PRO499, THR1053, HIS1054, THR1057, PHE1074	LEU1077
G1249R + Apoptozole	LEU1279, ARG1259, THR1278, LEU1187, ALA959, SER955, THR1176, GLU279, GLN1280	ILE1277, GLN1186, GLY1185, GLN958, PRO1175, PRO960, GLU278, LEU957
G1249R + Chromophore	GLU278, ARG1283, LEU1261, MET961, ARG1259, LEU1260, PRO960, TRP1274, LYS1177, ILE1277, THR1278, ASN1184, PRO1175, ASP1275, ALA595, THR1176, GLN958	LYS273, LEU1279
G1249R + Congo Red	VAL171, GLN179, SER182, ASN186, ASN187, ILE371, PHE374, ARG170, LYS370, GLN378	LYS174, LYS377, LEU183, ILE175, LYS370
G1249R + Melanin	SER422, ASN423, GLU424, PHE409, LYS411, ALA412, LYS413, GLU410, GLN414, ASN418	THR421, ALA412
G1249R + NAD	GLN958, LEU1260, MET961, ARG1259, PRO960, LEU1261, THR1263, ASN1262, SER962,THR1220, GLU1221, LYS1174, THR1776, GLU278, ALA959, LEU957	ARG1283, LYS273
G1249R + Nelfinavir	SER962, THR1278, ARG1283, LYS273, LEU957, GLU279, PRO1175, PRO960, MET961, LEU1261, ASN1262, SER962	LEU1279, ARG1259, GLU278
I105N + Apoptozole	GLU402, SER431, GLY437, ASP173, PHE430, SER176, LEU428	ARG170, LEU436, PHE405, SER431, TRP401, LYS174
I105N + Chromophore	ARG1283, GLU1221, ASN1262, THR1220, SER962, LEU1261, TRP1274, THR1278, ILE1277, ALA959, PRO1175, THR1176, LYS273, GLN958, PRO960	ARG1259, LEU1279
I105N + cAMP	ASN1262, MET961, ALA959, ARG1283, LYS273, GLN958, PRO1175, PRO960, LEU1260, LEU1261,	ARG1259

	THR1263, ASN126	
I105N + Congo Red	GLN958, HIS954, ASN1184, LYS1183, SER1276, ASP1275,ILE1277, GLN1280, LYS273, GLU282, GLU279	SER1188, LYS1177, GLU278, LEU957, THR1278
I105N + NAD	ARG1283, LEU1260, LEU1261, LEU1279, ASN1262, TRP1274, LYS1177, GLN1186, ASN1184, ALA959, GLN958, GLY1185, SER1188, SER1276, THR1278, MET961, PRO960, PRO1175	ILE1277, ARG1259
I105N + Cpd-β	CYS276, HIS954, GLU282, GLN958, LYS273, GLN1280, GLN1309, TYR1307	GLU279, LEU957, GLU278
K273Q + Apoptozole	GLN1280, ASP1275, THR1278, GLU278, GLN158, ALA959, THR1176, PRO960, ASN1262, LEU1261, LYS1177, ARG1259,MET96	TRP1274, ILE1277,PRO1175
K273Q + Chromophore	PHE430, GLN179, ASP373, LYS370, LEU183, LYS377, PHE374,VAL1171, ARG170, LEU428	LYS174, ILE175, PHE429
K273Q + Melanin	ILE175, PHE374, LYS377, LEU183, GLN179, SER182	ASP373, LYS370
K273Q + Congo Red	SER1178, LYS1180, GLY1185, PRO1175, ARG1259, LYS1177, GLN258, GLN273, ALA259, ARG1283, LEU1260	PRO960, THR1176, LEU1279, ASN1184, LYS1183
I105N + NAD	LEU957, PRO1175, GLN273, ARG1283, LEU1279, THR1278, SER118, PRO960, ARG1283, LEU1187, GLN273, ASN1184, LYS1177	TRP1274, ARG1259
K273Q + Nelfinavir	GLU278, GLU273, ARG1283, GLN958, MET961, SER1188, THR1278, LYS1177, GLN1280, TRP1274, ILE1277, ASN1275, SER1276, SER1188	PRO960, ILE1279

Chromophore exhibited extensive hydrogen bonding with residues such as ASN1262, SER962, LEU1260, ASP1275, ILE1277, TRP1274, LYS1177, THR1278, GLU1280, and GLN258 in wild-type CFTR, with hydrophobic contacts mainly at LEU1279 and ARG1259. In the G1249R mutant, chromophore formed hydrogen bonds with GLU278, ARG1283, LEU1261, MET961, ARG1259, LEU1260, PRO960, TRP1274, LYS1177, ILE1277, THR1278, ASN1184, PRO1175, ASP1275, ALA595, THR1176, and GLN958, and hydrophobic interactions at LYS273 and LEU1279. In I105N, it bound through hydrogen bonds with ARG1283, GLU1221, ASN1262, THR1220, SER962, LEU1261, TRP1274, THR1278, ILE1277, ALA959, PRO1175, THR1176, LYS273, GLN958, and PRO960, while hydrophobic interactions involved ARG1259 and LEU1279. For K273Q, chromophore mainly bound through hydrogen bonds with PHE430, GLN179, ASP373, LYS370, LEU183, LYS377, PHE374, VAL1171, ARG170, and LEU428, and showed hydrophobic contacts with LYS174, ILE175, and PHE429 (*Table 9*). Congo red in the wild type formed hydrogen bonds with ARG1259, LEU1260, LEU1279, TRP1274, SER1276, ASN1184, THR1278, ILE1177, LYS1177, SER962, GLU1221, ASN1262, LEU1261, MET961, and GLN1186, and hydrophobic associations with LEU1187 and PRO96. In the G1249R mutant, hydrogen bonds were observed with VAL171, GLN179, SER182, ASN186, ASN187, ILE371, PHE374, ARG170, LYS370, and GLN378, while hydrophobic contacts involved LYS174, LYS377, LEU183, and ILE175. In I105N, Congo red interacted through hydrogen bonds with GLN958, HIS954, ASN1184, LYS1183, SER1276, ASP1275, ILE1277, GLN1280, LYS273, GLU282, and GLU279, with hydrophobic associations at SER1188, LYS1177, GLU278, LEU957, and THR1278. In K273Q, hydrogen bonds were seen with SER1178, LYS1180, GLY1185, PRO1175, ARG1259, LYS1177, GLN258, GLN273, ALA259, ARG1283, and LEU1260, with hydrophobic interactions at PRO960, THR1176, LEU1279, ASN1184, and LYS1183 (*Table 9*).

Additionally, Cpd β bound wild-type CFTR through hydrogen bonds with SER1188, THR1278, THR1263, ASN1184, SER1276, ILE1222, TRP1224, LEU1260, SER962, and LEU1961, while hydrophobic contacts involved LEU1229, ARG1259, MET961,

PRO960, ASN1262, and LEU1229. In I105N, hydrogen bonding was observed with CYS276, HIS954, GLU282, GLN958, LYS273, GLN1280, GLN1309, and TYR1307, alongside hydrophobic contacts with GLU279, LEU957, and GLU278 (*Table 9*). Moreover, cAMP in the wild type showed hydrogen bonding with GLN378, LYS181, TYR380, SER168, GLU474, ARG170, LEU475, TRP401, SER478, and PRO477, and hydrophobic interactions with GLU476 and GLU403. In I105N, cAMP formed hydrogen bonds with ASN1262, MET961, ALA959, ARG1283, LYS273, GLN958, PRO1175, PRO960, LEU1260, LEU1261, THR1263, and ASN126, and a hydrophobic contact with ARG1259 (*Table 9*). Furthermore, Melanin bound wild-type CFTR through hydrogen bonds with TYR1073, GLU504, PRO499, THR1053, HIS1054, THR1057, and PHE1074, together with hydrophobic interactions involving LEU1077. In the G1249R mutant, melanin interacted through hydrogen bonds with SER422, ASN423, GLU424, PHE409, LYS411, ALA412, LYS413, GLU410, and GLN414, and hydrophobic associations with THR421 and ALA412. In the K273Q mutant, hydrogen bonding occurred with ILE175, PHE374, LYS377, LEU183, GLN179, and SER182, and hydrophobic contacts with ASP373 and LYS370. Finally, NAD interacted with wild-type CFTR through hydrogen bonds with GLN958, LEU1260, MET961, ARG1259, PRO960, LEU1261, THR1263, ASN1262, SER962, THR1220, GLU1221, LYS1174, THR1776, GLU278, ALA959, and LEU957, with hydrophobic associations at ARG1283 and LYS273. In the G1249R mutant, similar interactions were observed with key residues, while in I105N, NAD formed hydrogen bonds with ARG1283, LEU1260, LEU1261, LEU1279, ASN1262, TRP1274, LYS1177, GLN1186, ASN1184, ALA959, GLN958, GLY1185, SER1188, SER1276, THR1278, MET961, PRO960, and PRO1175, along with hydrophobic contacts with ILE1277 and ARG1259 (*Table 9*).

Such ligands showed strong docking scores with both wild-type and mutant CFTR proteins, suggesting their potential as scaffolds for CFTR modulators. Structure-based refinement, molecular dynamics, and functional assays are essential to validate these candidates and optimize their selectivity, stability, and pharmacokinetics. Promising compounds should progress to cellular and in vivo studies, with delivery strategies such as oral or inhaled formulations enhancing therapeutic relevance. Repurposed agents like nelfinavir may accelerate approval, while novel scaffolds will require extensive preclinical testing. An integrated pipeline combining computational, experimental, and regulatory approaches offers a path toward effective CFTR-targeted therapies. Cystic fibrosis (CF) is a common inherited multisystem disorder caused by CFTR mutations, affecting the respiratory, gastrointestinal, and reproductive systems. First linked to leukotriene production in 1981, CFTR was mapped to chromosome 7q31.2 in 1989 and characterized with 24 exons. Over 4,000 mutations have been reported, with F508del (~70% of alleles) being the most prevalent, alongside G542X, N1303K, G551D, and W1282X. Amino acid substitutions account for over 40% of variants, and SNPs are the main source of genetic diversity, cataloged in CFTR1 databases. Computational approaches help predict structural and functional impacts of CFTR mutations, allowing identification of high-risk nsSNPs for experimental validation and drug development. This study employed an integrated computational strategy to evaluate CFTR nsSNPs and identify potential therapeutic modulators. Multiple tools were used to predict pathogenicity, disease association, stability, residue conservation, and post-translational modifications. Homology models of wild-type and mutant CFTR were built and validated with SWISS-MODEL, ModRefiner, SAVES, Ramplot, QMEAN, and TM-align, while HOPE analyzed physicochemical effects of substitutions. Molecular

docking with PyRx (AutoDock Vina) using PubChem and literature-sourced ligands revealed altered interactions in mutant proteins. The findings highlight high-risk nsSNPs that destabilize CFTR, disrupt ligand binding, and provide targets for experimental validation and drug development.

From an initial dataset of 282,490 SNPs, 10,618 were non-synonymous, indicating potential functional relevance. SIFT and PolyPhen consistently predicted 132 nsSNPs as deleterious, forming a high-confidence subset. Further analyses with SNAP2, PROVEAN, CADD, ConDEL, SNPs&GO, P-Mut, PhD-SNP, and Meta-SNP largely confirmed their pathogenicity, with few variants consistently neutral. Protein stability predictions using i-Mutant 3.0, MUPro, and i-Stable showed that 106 nsSNPs reduce CFTR stability. CONSURF analysis revealed 98 variants in highly conserved residues, 46 of which scored maximally, emphasizing functional importance. Post-translational modification predictions identified C524, S707, and S737 as potentially affecting CFTR activity. Thirty nsSNPs were prioritized for structural analysis based on consistent deleterious predictions across 15 algorithms. Available PDB structures are partial, often representing only wild-type CFTR, while disease-relevant mutations like I105N, K273Q, and G1249R are absent. Notably, PDB 6MSM depicts ATP-bound, phosphorylated CFTR, 5UAK shows NBD1 with regulatory elements, and 5W81 includes NBD1 with F508del, illustrating mutation-induced structural disruptions. Homology modeling with SWISS-MODEL enabled generation of complete, mutation-specific CFTR structures with structural refinement and energy minimization. Using Q2IBA1.1.A (CFTR_CHLAE) as a template, the model achieved 98.31% sequence identity and a GMQE of 0.76. Refinement via ModRefiner and validation with SAVES showed 96.2% of residues in favorable conformations (ProCheck), an ERRAT score of 97.524, Verify3D acceptability of 52.39%, and a QMEAN4 of –3.29, confirming reliability. TM-align indicated that I105N, K273Q, and G1249R had the highest RMSD values (0.93–0.98 Å), reflecting notable conformational changes. HOPE analysis revealed substitutions affecting size, charge, and hydrophobicity, likely impacting stability and function. Ramachandran analysis in 2D and 3D confirmed most torsion angles in favored or allowed regions, with minimal residues in disallowed regions, validating stereochemical integrity.

Molecular docking predicts interactions between ligands and target proteins, providing insights into binding affinity, specificity, and potential biological activity. Docking against CFTR and its variants identified ligands with strong modulatory potential, including apoptozole, chromophore, Congo Red, cpd β, cAMP, NAD, Nelfinavir, and melanin. cAMP enhances CFTR activity via PKA-mediated phosphorylation, while phenothiazine and chlorpromazine influence channel gating and trafficking. Antiviral agents like amprenavir and nelfinavir may aid misfolded CFTR rescue by modulating protein folding and ER stress, and apoptozole, an Hsp70 inhibitor, may improve CFTR stabilization. Congo Red and chromophores likely act as chemical chaperones, stabilizing misfolded conformations. Natural metabolites such as NAD, biotin, hyaluronic acid, and melanin may support CFTR stability through redox regulation, energy metabolism, and antioxidant effects. These findings highlight diverse ligands with potential for rescuing defective CFTR and guiding drug repurposing and novel modulator discovery for cystic fibrosis therapy. Our results showed that Chromophore (–9.1 kcal/mol) and apoptozole (–9.0 kcal/mol) had the highest binding affinities, suggesting strong potential to stabilize CFTR. Congo Red, amprenavir, and nelfinavir exhibited moderate binding (–6.2 to –7.8 kcal/mol), consistent with roles in

protein folding and stress response modulation, while cAMP (–7.0 to –8.0 kcal/mol) reinforced its known PKA-mediated activation of CFTR. Natural cofactors, including NAD, biotin, hyaluronic acid, and melanin, displayed favorable binding (–5.1 to –8.7 kcal/mol) and maintained interactions across all variants (–8.3 to –8.6 kcal/mol), indicating potential contributions to CFTR stabilization through metabolic or antioxidant mechanisms. Detailed interaction analysis revealed extensive hydrogen bonds and hydrophobic contacts with key residues. For example, apoptozole engaged GLN376, LEU375, and LYS162 in the wild type, and LEU1279, ARG1259, and THR1278 in the G1249R mutant. Chromophore, Congo Red, cpd β, cAMP, NAD, and melanin similarly formed stable interactions within CFTR pockets, highlighting promising scaffolds for drug discovery and repurposing. Translating these findings to therapeutics will require electrophysiological assays, protein folding studies, molecular dynamics, and binding free energy analyses. ADMET profiles are generally favorable, though solubility, stability, and inhaled delivery may need optimization. Repurposed drugs like nelfinavir and amprenavir could advance rapidly, whereas novel scaffolds such as apoptozole or chromophore derivatives will require extensive preclinical evaluation. The identified binding sites align with Odolczyk's findings, highlighting two NBD1 pockets and residues F494, W496, K1060, and W1063 as critical for corrector activity. Confirmation via site-directed mutagenesis and validation with molecular dynamics and free energy calculations is necessary. While CFTR-targeted therapies like ivacaftor and VX-809 improve survival, longer lifespans introduce new risks, including cancer susceptibility, reflecting CFTR's broader roles in growth, differentiation, and regeneration. Computational predictions must therefore be integrated with mutational, biophysical, and clinical studies to refine therapies and guide genetic counseling.

Conclusion

This study applied an in-silico pipeline to assess deleterious CFTR nsSNPs and identify potential modulators through molecular docking. We found that 30 nsSNPs were predicted as highly deleterious, with I105N, K273Q, and G1249R showing major destabilizing effects on CFTR structure and function. Docking revealed strong ligand affinities, notably for apoptozole, chromophore, Congo Red, NAD, melanin, and cAMP, while repurposed drugs such as nelfinavir and amprenavir also showed promising interactions. These results highlight key pathogenic variants and suggest opportunities for drug repurposing and modulator development, providing a foundation for experimental validation and personalized therapies in cystic fibrosis.

Acknowledgement

The authors acknowledge the use of freely available databases and computational tools that enabled this research.

Conflict of interest

The authors confirm that there is no conflict of interest involve with any parties in this research study.

REFERENCES

[1] AbdulAzeez, S., Borgio, J.F. (2016): In-silico computing of the most deleterious nsSNPs in HBA1 gene. – PloS One 11(1): 13p.

[2] Abuzaid, O., Idris, A.B., Yılmaz, S., Idris, E.B., Idris, L.B., Hassan, M.A. (2024): Prediction of the most deleterious non-synonymous SNPs in the human IL1B gene: evidence from bioinformatics analyses. – BMC Genomic Data 25(1): 15p.

[3] Adeniji, S.E., Uba, S., Uzairu, A. (2020): In silico study for evaluating the binding mode and interaction of 1, 2, 4-triazole and its derivatives as potent inhibitors against Lipoate protein B (LipB). – Journal of King Saud University-Science 32(1): 475-485.

[4] Armon, A., Graur, D., Ben-Tal, N. (2001): ConSurf: an algorithmic tool for the identification of functional regions in proteins by surface mapping of phylogenetic information. – Journal of Molecular Biology 307(1): 447-463.

[5] Aslam, T., Tariq, H., Saleem, M., Ramzan, K., Aaliya, K., Qadri, A.A.A.M., Zulfiqar, M. (2024): Bioinformatic Analysis of Human TLR4 Coding Variations Associated with Ocular Infection: A Structural Prediction and Molecular Docking Studies. – International Journal of Pharmaceutical Sciences 2(12): 930-954.

[6] Bilal, I., Munir, H., Ramzan, K., Zulfiqar, I., Waheed, A., Haider, A., Ali, F. (2025a): STRUCTURAL MODELING AND FUNCTIONAL PREDICTION OF IFN-Y GENE VARIANTS. – Quantum Journal of Medical and Health Sciences 4(3): 84-102.

[7] Bilal, I., Ramzan, K., Ramzan, S., Zulfiqar, M., Tahir, U., Moazzam, A., Haider, I. (2025b): Homology Modeling and Structural Docking Analysis on a Human BDNF Gene by Using Computational Algorithms. – Journal of Advances in Biology & Biotechnology 28(4): 464-487.

[8] Chandrasekaran, G., Hwang, E.C., Kang, T.W., Kwon, D.D., Park, K., Lee, J.J., Lakshmanan, V.K. (2017): Computational Modeling of complete HOXB13 protein for predicting the functional effect of SNPs and the associated role in hereditary prostate cancer. – Scientific Reports 7(1): 18p.

[9] Deletang, K., Taulan-Cadars, M. (2022): Splicing mutations in the CFTR gene as therapeutic targets. – Gene Therapy 29(7): 399-406.

[10] George Priya Doss, C., Rajasekaran, R., Sudandiradoss, C., Ramanathan, K., Purohit, R., Sethumadhavan, R. (2008): A novel computational and structural analysis of nsSNPs in CFTR gene. – Genomic Medicine 2(1): 23-32.

[11] Hasnain, M.J.U., Shoaib, M., Qadri, S., Afzal, B., Anwar, T., Abbas, S.H., Sarwar, A., Talha Malik, H.M., Tariq Pervez, M. (2020): Computational analysis of functional single nucleotide polymorphisms associated with SLC26A4 gene. – PLoS One 15(1): 20p.

[12] Hasan, M.M., Khatun, M.S. (2018): Prediction of protein post-translational modification sites: an overview. – Ann Proteom Bioinform 2: 049-057.

[13] Heidarinia, H., Tajbakhsh, E., Bahrami, Y., Rostamian, M. (2025): Design a multi-epitope vaccine candidate against Acinetobacter baumannii using advanced computational methods. – AMB Express 15(1): 23p.

[14] Ideozu, J.E., Liu, M., Riley-Gillis, B.M., Paladugu, S.R., Rahimov, F., Krishnan, P., Tripathi, R., Dorr, P., Levy, H., Singh, A., Waring, J.F. (2024): Diversity of CFTR variants across ancestries characterized using 454,727 UK biobank whole exome sequences. – Genome Medicine 16(1): 14p.

[15] Kumar, M., Rathore, R.S. (2025): RamPlot: a webserver to draw 2D, 3D and assorted Ramachandran (φ, ψ) maps. – Applied Crystallography 58(2): 630-636.

[16] Kumari, A., Mittal, I., Kaushik, A., Jaitly, A., Nain, N., Toor, D.S., Pal, T., Saini, S., Thakur, C.J. (2025): A comprehensive computational study of non-synonymous SNPs (nsSNPs) of NTRK1 Gene using conservation, stability, docking, and simulation approaches. – In Silico Research in Biomedicine 13p.

[17] López-Ferrando, V., Gazzo, A., De La Cruz, X., Orozco, M., Gelpí, J.L. (2017): PMut: a web-based tool for the annotation of pathological variants on proteins, 2017 update. – Nucleic Acids Research 45(W1): W222-W228.
[18] Magesh, R., George Priya Doss, C. (2014): Computational pipeline to identify and characterize functional mutations in ornithine transcarbamylase deficiency. – 3 Biotech 4(6): 621-634.
[19] Mathew, A., Dirawi, M., Abou Tayoun, A., Popatia, R., Aldirawi, M. (2021): A rare cystic fibrosis transmembrane conductance regulator (CFTR) mutation associated with typical cystic fibrosis in an Arab child. – Cureus 13(2): 4p.
[20] Parisi, G.F., Mòllica, F., Giallongo, A., Papale, M., Manti, S., Leonardi, S. (2022): Cystic fibrosis transmembrane conductance regulator (CFTR): Beyond cystic fibrosis. – Egyptian Journal of Medical Human Genetics 23(1): 10p.
[21] Purushothaman, A.K., Nelson, E.J.R. (2023): Role of innate immunity and systemic inflammation in cystic fibrosis disease progression. – Heliyon 9(7): 16p.
[22] Rafique, H., Safdar, A., Ghani, M.U., Akbar, A., Awan, F.I., Naeem, Z., Amar, A., Awan, M.F., Wajahat Ullah, S., Shaikh, R.S. (2024): Exploring the diversity of CFTR gene mutations in cystic fibrosis individuals of South Asia. – Journal of Asthma 61(6): 511-519.
[23] Ramananda, Y., Naren, A.P., Arora, K. (2024): Functional consequences of CFTR interactions in cystic fibrosis. – International Journal of Molecular Sciences 25(6): 35p.
[24] Ramzan, K., Noman, A. (2024): Structural Analysis And Protein-Ligand Docking Approach Of BrainAssociated APOE, SNCA, And PRKN Genes. – International Journal of Pharmaceutical Sciences 2: 393-410.
[25] Rasheed, A., Safdar, M., Umar, A., Khan, M.S., Ramzan, S., Ramzan, K., Sabri, S., Shaffique, S., Tahir, M.Z. (2025): Comparative bioinformatics analysis and functional characteristics of natriuretic peptide B (NPPB) gene in humans. – In Silico Research in Biomedicine 13p.
[26] Tariq, H., Asif, M., Saleem, M., Ramzan, K., Zulfiqar, M., Amir, A., Asif, A.R. (2024): Evaluation of Detrimental Missense SNPs of Human CXCL6 Gene by Combining Algorithms, Homology Modeling, and Molecular Docking. – Inventum Biologicum: An International Journal of Biological Research 4(4): 92-106.
[27] Venkata Subbiah, H., Ramesh Babu, P., Subbiah, U. (2020): In silico analysis of non-synonymous single nucleotide polymorphisms of human DEFB1 gene. – Egyptian Journal of Medical Human Genetics 21(1): 9p.
[28] Waheed, S., Ramzan, K., Ahmad, S., Khan, M.S., Wajid, M., Ullah, H., Umar, A., Iqbal, R., Ullah, R., Bari, A. (2024): Identification and In-Silico study of non-synonymous functional SNPs in the human SCN9A gene. – PloS One 19(2): 22p.
[29] Wang, D., Liu, D., Yuchi, J., He, F., Jiang, Y., Cai, S., Li, J., Xu, D. (2020): MusiteDeep: a deep-learning based webserver for protein post-translational modification site prediction and visualization. – Nucleic Acids Research 48(W1): W140-W146.
[30] Zhang, B., Zhang, Y., Zhang, Y., Liu, X., Zhang, R., Wang, Z., Pan, F., Xu, N., Shao, L. (2025): Identified five variants in CFTR gene that alter RNA splicing by minigene assay. – Frontiers in Genetics 16: 9p.